Universidade de Aveiro
2016

Departamento de Física

Pedro Miguel
Fernandes Correia

Simulação de efeitos de esteira distante gerados por parques eólicos offshore usando o modelo WRF: O caso de estudo de Horns Rev.

Simulation of far wake effects generated by offshore wind farms using the WRF model: The Horns Rev test case.

Dissertação apresentada à Universidade de Aveiro para cumprimento dos requisitos necessários à obtenção do grau de Mestre em Meteorologia e Oceanografia Física, realizada sob a orientação científica do Prof. Doutor José Castanheira, Professor do Departamento de Física da Universidade de Aveiro

Parte deste trabalho foi desenvolvido no *CENER*, inserido no projecto Europeu *EERA-DTOC*.

CENER | NATIONAL RENEWABLE ENERGY CENTRE
ADItech

EERA DTOC
THE EUROPEAN ENERGY RESEARCH ALLIANCE
DESIGN TOOLS FOR OFFSHORE WIND FARM CLUSTER

o júri / the jury

Presidente	**Doutor Alfredo Rocha** Professor Associado com Agregação do Departamento de Física da Universidade de Aveiro
Vogais	**Doutor Rui Paulo Vasco Salgado** Professor Auxiliar do Departamento de Física da Universidade de Évora
	Doutor José Manuel Castanheira Professor Auxiliar do Departamento de Física da Universidade de Aveiro

Agradecimentos

Quero agradecer primeiro ao CENER por me ter permitido realizar este mestrado, tanto ajudando-me monetariamente no pagamento das propinas, assim como facilitando em algumas ocasiões que me deslocasse a Portugal para realizar exames e reunir-me com o orientador desta dissertação. Também não posso deixar de agradecer a ajuda e apoio dos meus companheiros de trabalho Roberto, Sergio e Elena que sempre me deram uma ajuda quando necessitava e que sempre se mostraram disponíveis para dar o seu conselho e esclarecer as mais variadas dúvidas durante a realização deste trabalho. Agradeço também ao meu orientador todo o apoio, conselhos e o precioso tempo que dedicou para que o esta dissertação pudesse reflectir da melhor maneira todo o trabalho que foi realizado. Apesar de a comunicação à distância ser sempre complicada, nunca deixei de sentir o seu apoio e boa vontade de solucionar todos os pequenos problemas que sempre iam surgindo. A todos o meu muito obrigado.

Palavras Chave / Keywords

Far wake effects, WRF, wind farm parameterization, wind speed deficit, Horns Rev, offshore

Resumo / Abstract

Avanços tecnológicos e científicos contínuos contribuíram para a melhoria da relação custo/benefício na exploração de energia eólica offshore. Esses avanços levaram ao aumento do número e tamanho de novos parques eólicos offshore. O crescente número de parques em algumas zonas leva a que surjam áreas com uma alta concentração de parques eólicos, algumas delas dentro da raio de influência de outros parques situados na sua vizinhança. Devido à proximidade entre parques, estes podem funcionar como um obstáculo para o fluxo normal do vento e afectar a velocidade do vento noutros parques situados a jusante. Efeitos de esteira distante provocados pelo efeito combinado de efeitos de esteiras de turbinas e de clusters ou parques individuais podem originar deficits de velocidade significativos numa grande área ao redor de uma zona de interesse. O estudo das interacções entre parques eólicos e as resultantes perdas por efeito de esteira em parques eólicos vizinhos é um aspecto importante que deve ser tido em conta quando se decide o "layout" e localização de novos parques offshore.

Devido às condições favoráveis para a exploração de energia eólica offshore no Mar de Norte, a concentração de parques eólicos nessa região é alta e continua a aumentar tornando-a uma zona indicada para este tipo de estudo. Quando se considera uma área destas dimensões, o tamanho do domínio e a resolução horizontal podem tornar-se num obstáculo difícil de ultrapassar. Devido a que os modelos actuais usados para o estudo de efeito de esteira necessitam de um poder computacional bastante elevado, é bastante difícil simular áreas com centenas de quilómetros de comprimento que englobam vários parques eólicos offshore com diferentes áreas, características e tipo de turbinas eólicas.

A recente implementação de parameterizações de parques eólicos no código fonte de modelos de mesoscala pode constituir uma ferramenta indispensável para ultrapassar estes obstáculos. Usando o modelo de mesoscala *Weather Research and Forecasting* (WRF), que inclui uma parameterização de parque eólico, simularam-se os parques eólicos offshore de Horns Rev 1 e Horns Rev 2. Este trabalho tenta quantificar o deficit de velocidade no parque de Horns Rev 1 devido à construção do parque de Horns Rev 2 na vizinhança do mesmo. Uma validação dos resultados é efectuada usando dados medidos de várias torres situadas na zona do parque de Horns Rev 1, e uma análise do potencial desta metodologia é efectuada.

Palavras Chave / Keywords

Far wake effects, WRF, wind farm parameterization, wind speed deficit, Horns Rev, offshore

Resumo / Abstract

Continuous technological and scientific advances have contributed to the improvement of the relation cost-benefit in the exploitation of offshore wind farms. Those advances have propelled the construction of new and larger offshore wind farms and have contributed to a high concentration of wind farms in several areas, some of them built within the radius of influence of other neighbour wind farms. Because of their proximity, some of them might impact the wind conditions on other downstream plants. Pronounced far wakes effects generated by the combination of individual wind turbines and single or clusters of wind farms can provoke significant wind speed deficits within a large radius around a given location. The study of these wind farm interactions and the resulting wake losses on neighbouring wind farms is an important aspect that should be taken into account when deciding the layout and location of new offshore plants.

Due to its favourable conditions to wind energy exploitation, the concentration of offshore wind farms in the North Sea region is high and it is still increasing making it a suitable location for this study. When considering such a large area, the domain size and resolution of the numerical models might be an obstacle difficult to overcome. Since current wake models require high computational power, it is very difficult to simulate areas with hundreds of kilometres and several wind farms with different sizes, characteristics and different types of turbines.

The recent implementations of wind farm parameterizations in the source code of mesoscale models could provide the required tool to overcome those constraints. Using the state of the art *Weather Research and Forecasting* (WRF) mesoscale model, that includes a wind farm parameterization scheme, the Horns Rev 1 and Horns Rev 2 wind farms are simulated. This work tries to ascertain the wind speed deficits in the Horns Rev 1 wind farm due to the construction of the Horns Rev 2 plant in its proximity. An evaluation of the results is performed against real measurements from the site and the capabilities of the methodology are discussed.

CONTENTS

List of Figures

List of Tables

ACRONYMS

ANOVA	Analysis of variance. 9, 27
BAMS	Best Annual Mean and Standard Deviation. 9, 26, 30, 31
CENER	National Renewable Energy Center. 9, 17, 22, 56
CFD	Computational Fluid Dynamics. 9, 20–22
DTU	Technical University of Denmark. 9, 16, 38
EERA-DTOC	Design Tools for Offshore Wind Farm Cluster. 9, 17, 24, 56
EOF	Empirical Orthogonal Functions. 9
GCM	Global Circulation Models. 9, 26
HR	Horns Rev. 9, 16, 17, 32, 33, 35, 42
HR1	Horns Rev 1. 8, 9, 16, 17, 20, 32, 33, 35, 36, 43–56
HR2	Horns Rev 2. 8, 9, 16, 32, 33, 35, 43, 45, 47–50, 54–56
KE	Kinetic Energy. 9, 23, 24
MAE	Mean Absolute Error. 9, 40, 42
MERRA	Modern-Era Retrospective Analysis for Research and Applications. 9, 28, 29
MSLP	Mean Sea-Level Pressure. 9, 26, 28–30
MYNN	Mellor-Yamada-Nakanishi-Niino. 9, 33, 34
PBL	Planetary Boundary Layer. 9, 22, 33, 34
PCA	Principal Component Analysis. 6, 9, 26, 28, 29, 31
RAE	Relative Absolute Error. 9, 31
RMSE	Root Mean Square Error. 9, 30, 40, 42

SAR Synthetic Aperture Radar. 9, 17, 24, 25

SOM Self-Organizing Maps. 9, 26, 28, 31

TKE Turbulent Kinetic Energy. 9, 24, 33

WRF Weather Research and Forecasting. 9, 16, 17, 21–25, 31–34, 40, 43–46, 54, 56

LIST OF SYMBOLS

Symbol	Description	Unit
A	Area obtained from turbine diameter	m^2
ρ	Air density	$kg\,m^{-3}$
α	Constant related to thrust coefficient	
β	Wake expansion parameter	
c	Constant related to *Prandtl* mixing length	
C_p	Power coefficient	
C_t	Thrust coefficient	
D	Turbine diameter	m
D_w	Rotor wake diameter	m
$\mathbf{F}_{Drag}$	Force of drag induced by wind turbine	N
K	Wake decay coefficient	
$\mathbf{N_t^{ij}}$	Number of turbines per square meter	
$\mathbf{N}$	Number of records	
p_d^-	Downstream pressure	Pa
p_d^+	Upstream pressure	Pa
P_∞	Freestream pressure	Pa
r	Radial distance	m
s	Normalized distance to rotor diameter	m
U_∞	Freestream wind speed	$m\,s^{-1}$
U_0	Incident wind speed	$m\,s^{-1}$

Symbol	Description	Unit
$\mathbf{V}$	Horizontal velocity vector	$\mathrm{m\,s^{-1}}$
$\mathbf{W_{meas.}}$	Measured wind speed	$\mathrm{m\,s^{-1}}$
$\mathbf{W_{sim.}}$	Simulated wind speed	$\mathrm{m\,s^{-1}}$
$\mathbf{z_{k+1}}$	Height at model level $k+1$	m
$\mathbf{z_{k}}$	Height at model level k	m

CHAPTER 1

INTRODUCTION

1.1 OBJECTIVE

The number and sheer size of offshore wind farms is increasing. Continuous technological and scientific advances have contributed to the improvement of the relation cost-benefit in the exploitation of offshore wind energy making it a desired target for investment. The general improvement in the Global economy and the renewed confidence in the sector after the 2008 financial crisis lead to a significant increase in offshore installed net capacity in 2015.

Accordingly with the last *European Wind Energy Association* (EWEA) report (Ho et al., 2016) for the year 2015, 3019MW of net capacity were installed and connected to the grid, which represented an increase of 108% over 2014. There are now 11027MW of total net capacity in Europe, resulting from 3.230 wind turbines installed and connected to the electrical grid. Another 6 mega projects are underway and once finished, an additional 1.9GW will be available, reaching a total of 12.96GW installed wind power capacity.

The *Horizon 2020*[1] program aimed to obtain 40GW of installed wind energy capacity for 2020 and 150GW for 2030. There is still a long road ahead to achieve this ambitious goal and an even bigger increase in the number and size of offshore wind farms and wind turbines is expected in the nearest future.

Since the first offshore wind farm built in the early nineties in Denmark [2] that was composed of eleven 450kW wind turbines, the offshore energy industry has suffered an incredible evolution. As figure 1.1.1 indicates, the installed wind power capacity in Europe, in the last 10 years have been increasing almost exponentially. Fabricators are making bigger wind turbines available, which allied with the experience acquired throughout the years, makes it possible to build bigger wind farms by minimizing the risks and maximizing the return on the investment. Figure 1.1.2 shows the average size of offshore wind farms over the years. The tendency to build larger wind farms is clearly visible.

Due to its favourable conditions to wind energy exploitation, the concentration of offshore wind farms in the North Sea region is high (figure **??**) and keeps increasing. This have

[1] https://ec.europa.eu/programmes/horizon2020

[2] **Vindeby :** http://www.4coffshore.com/windfarms/vindeby-denmark-dk06.html

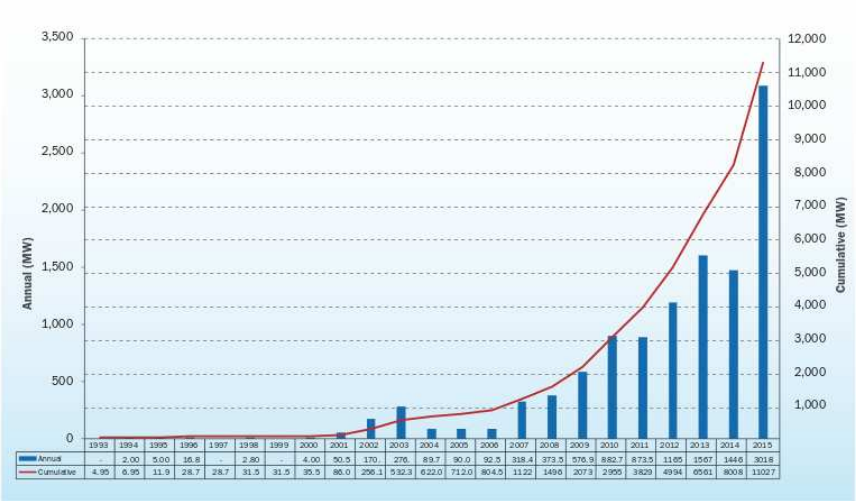

Figure 1.1.1: Evolution of the installed wind power capacity in Europe(MW) extracted from the technical report by Ho et al., 2016.

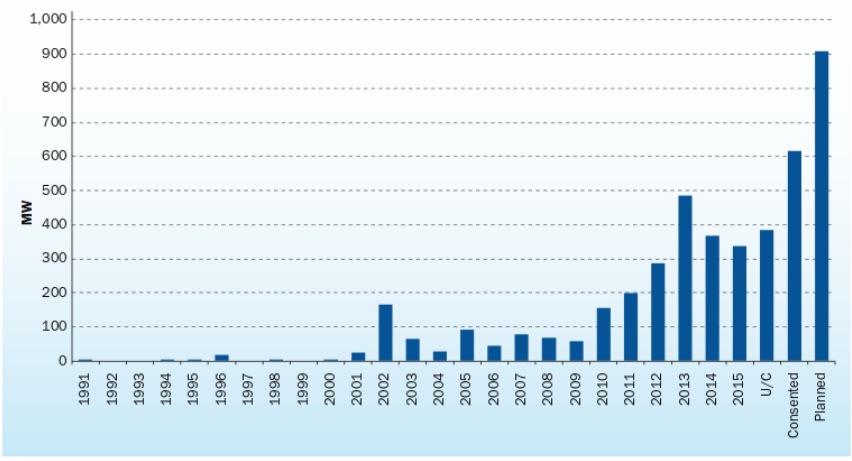

Figure 1.1.2: Average size of offshore wind farms extracted from the technical report by Ho et al., 2016.

contributed to a high concentration of offshore wind farms in several areas, some of them, built within the radius of influence of its neighbour wind farms (figure 1.1.4). That proximity, combined with certain meteorological conditions, might affect the wind conditions on other downstream plants. Pronounced far wakes effects generated by the combination of individual wind turbines and single or clusters of wind farms can provoke significant wind speed deficits within a large radius around a given location. The study of these wind farm interactions and the resulting wake losses on neighbouring wind farms is an important aspect that should be taken into account when deciding the layout and location of new offshore wind farms.

The simulation of the expected losses due to wake effects are usually carried away using a vast array of numerical models. Depending on the number of neighbour wind farms that could potentially affect the wind conditions at a given location, it might be necessary to simulate a

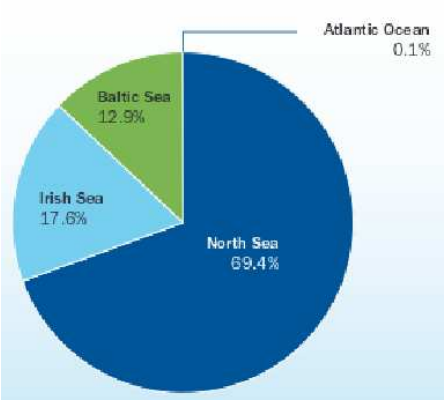

Figure 1.1.3: Installed wind power capacity by Sea basin, extracted from the technical report by Ho et al., 2016.

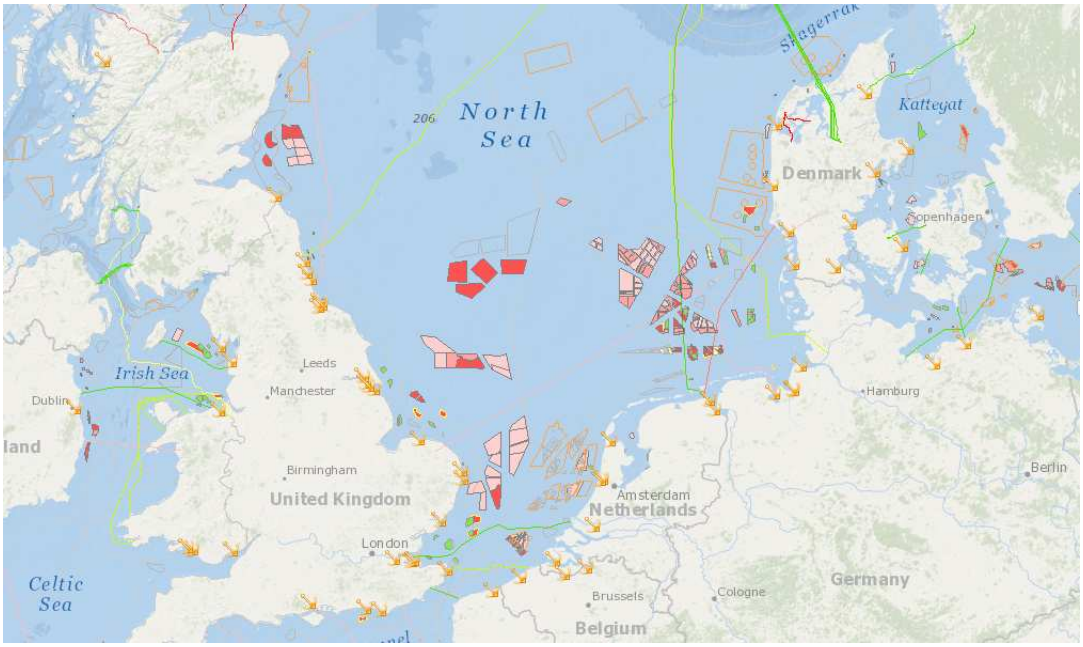

Figure 1.1.4: Offshore wind farm locations in the North Sea region. The installed and fully operational wind farms appear represented with the color green, under construction wind farms are shown in yellow, authorized for construction in red and the concept/early planning projects are shown in pink (Ho et al., 2016).

relatively big area. When considering such dimensions, the domain size and resolution of the numerical models might be an obstacle difficult to overcome. Since current wake models require high computational power, it is very difficult to simulate areas with hundreds of kilometres containing several offshore wind farms with different sizes, characteristics and different types of turbines.

Due to the implementation of wind farm parameterizations in the most recent versions, mesoscale models could provide a solution to overcome those constraints. Using the state of the art Weather Research and Forecasting (WRF) mesoscale model that includes a wind farm parameterization scheme (Fitch et al., 2012), the Horns Rev (HR) wind farm is simulated. HR

is located West of the coast of Denmark and it is constituted by two fully operational wind farms (HR1 and HR2). The first wind farm was built in 2002 with 80 wind turbines and the second was built in 2009 and has 91 wind turbines.

This particular wind farm was chosen because it suffered an enlargement that culminated in the construction of the HR2 wind farm. Analysing the measurements from the HR1 site, before and after the construction of the adjacent wind farm, it is possible to evaluate the mesoscale model capability of simulating far wake effects and try to ascertain their importance in the wind conditions of this particular offshore wind farm. Another important aspect is that this particular wind farm is one of the first large scale operating offshore wind farm in the World. It possesses three masts with several years of measured data at multiple heights, making it an invaluable tool to validate offshore methodologies knowing how extremely difficult it is to find reliable measurements.

Kurt Hansen, senior researcher at Technical University of Denmark (DTU), compiled and made available a database of measurements from the HR1 wind farm, including wind power from all the individual wind turbines for the period between 2005 and 2009. This data can be useful to determine if this methodology can go beyond the study of the wind speed deficit provoked by the far wake effects and provide a rough estimation on wind energy production for a given wind farm.

The main goal of the methodology presented in this dissertation, is to obtain a relatively "low-cost"[3] tool that could be used to perform a first analysis of an area of interest. This analysis includes the wind resource assessment simulation and the study of the wake effects produced by neighbour offshore wind farms that might affect the target area.

Some studies, regarding the use of mesoscale models to predict far wake effects in offshore wind farms, have already been made (Hasager et al., 2015) included in the European project Design Tools for Offshore Wind Farm Cluster (EERA-DTOC)[4]. This project was constituted by several European companies and universities and in one of its work packages, proposed to conduct an analysis of the state of the art methodologies and numerical models used to simulate offshore wake effects.

All the companies involved used their own methodologies and models to simulate a series of pre-determined test cases. The test cases were chosen based on a database of Synthetic Aperture Radar (SAR) imagery from several offshore wind farms in which it was possible to observe far wake effects. Comparisons between the several companies mesoscale methodologies outputs and the SAR images were performed but no validation against real measurements was made at the time.

One of the companies present at the EERA-DTOC project was the National Renewable Energy Center (CENER). A methodology using the WRF model and its wind farm parameterization was developed, constituting the basis for this work. By taking advantage of the available measurements at the HR wind farm this work further explores the capabilities of the

[3] Low cost refers to low computational cost when compared with standard microscale wake models. The lower computational requirements directly contribute to obtain a cheaper and faster tool.

[4] http://www.eera-dtoc.eu

developed methodology by properly validating the far wake effects on downstream wind speeds. Also, by having available wind power measurements from the HR1 wind farm, this work tries to ascertain if this methodology could be used to obtain a rough estimation of the theoretical wind power production of the wind farm, taking into account the far wake effects and its layout.

1.2 OUTLINE

The current study consists in using the WRF with the wind farm parameterization implemented in its source code to simulate the far wake effects generated by two neighbour wind farms. The results are validated against real measurements to confirm if this methodology can be used to predict far wake effects on other downstream offshore wind farms and if it possible to provide a rough estimation of the expected power loss due to those wake effects.

In chapter 2 it is given a brief introduction to wind turbine wakes as well as models and methodologies used to calculate them. A more detailed description of the proposed methodology is presented in the third chapter, while the chapter 4 presents the test case to be simulated. Finally, chapter 5 presents all the results obtained during the elaboration of this study.

CHAPTER 2

CONCEPTS OF WIND TURBINE WAKES AND WAKE MODELS

2.1 WAKE EFFECTS

As air flows through a wind turbine and energy is extracted, a wake is formed behind the rotor. A wind turbine wake refers to the stream-flow area affected by the presence of the wind turbine rotor. Inside this area occurs a diminution of axial wind speed, a sudden increase in static pressure and an increase in the turbulence intensity that leads to an expansion of the area in which the air flows (figure 2.1.1).

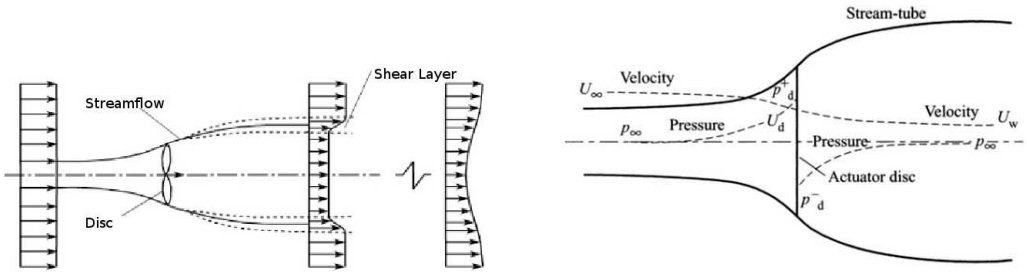

Figure 2.1.1: Scheme of a wake generated by a wind turbine (Jimenez et al., 2008).

Every wind turbine generates a downstream wake that provokes a decrease in wind speed and an increase in turbulence. If another wind turbine is placed downstream, within the distance of influence of this wake, its energy yield will be lower and the wind turbine loads[1] will be higher, resulting in a lower power production and a shorter lifespan of the machine. Over the ocean, wakes are even more significant than over land, often because wind turbines and wind farm sizes are bigger, there is no topography affecting the wake and in determined meteorological and atmospheric stability conditions, the combined wakes from a single or

[1] **Fatigue Loads:** Wind turbines are subject to fluctuating winds, and hence fluctuating forces, specially if they are located in a very turbulent wind climate. Components which are subject to repeated bending, such as rotor blades, may eventually develop cracks which ultimately may make the component break.

cluster of wind farms can spread for dozens or hundreds of kilometres (figure 2.1.2).
As described in section 1.1, the study of wake effects takes an even more significant role nowadays due to wind turbines and offshore wind farms growing larger and at the same time, new offshore wind farms projects are being planned or already undergoing construction. The increasing concentration of wind farms in several regions creates an increasing necessity to accurately describe the wind speed, wind shear and turbulence conditions at the client's area of interest.

Figure 2.1.2: Wake effects behind offshore wind turbines at the HR1 wind farm (Hasager et al., 2013). In these photos it's very easy to observe how the generated wakes span to other downstream wind turbines.

Depending on the type of study to be performed and the type of model to be used, a division between near and far wakes effects can be made. Generally a wind turbine wake can be divided in three main regions, depending on the distance to the rotor and wake characteristics (figure 2.1.3). The near wakes refer to the area, generally up to two or three rotor diameters behind the rotor, where that same rotor can be discriminated. The intermediate region is usually located between three and six rotor diameters, even though this distances may vary. Finally, the far wakes occur in the region beyond the intermediate wake, where the focus is put on the influence of wind turbines in farm situations and the modelling of the actual rotor is less important. In the far wake region it is assumed that the tip vortices, turbulence and vorticity generated at the individual rotors have been dissipated and the flow is smoother than in the near wake region.

2.1.1 Near Wakes

In near wake effects, aspects like number of blades and its aerodynamics, rotor and tip vortices are very important aspects to take into account. In order to simulate these phenomena, very high resolution models have to be employed. The main focus of these models are wake and turbulence effects from singular wind turbines and blade aerodynamics. The near wake is characterized by a wake expansion, a decrease in the axial velocity and an increase in the static pressure and turbulence. Figures 2.1.1 and 2.1.3 illustrate the behaviour of the wind turbine wake.
Several type of microscale models are used to obtain near wake effects. Some are empirical/analytical models while other are based on Computational Fluid Dynamics (CFD) .

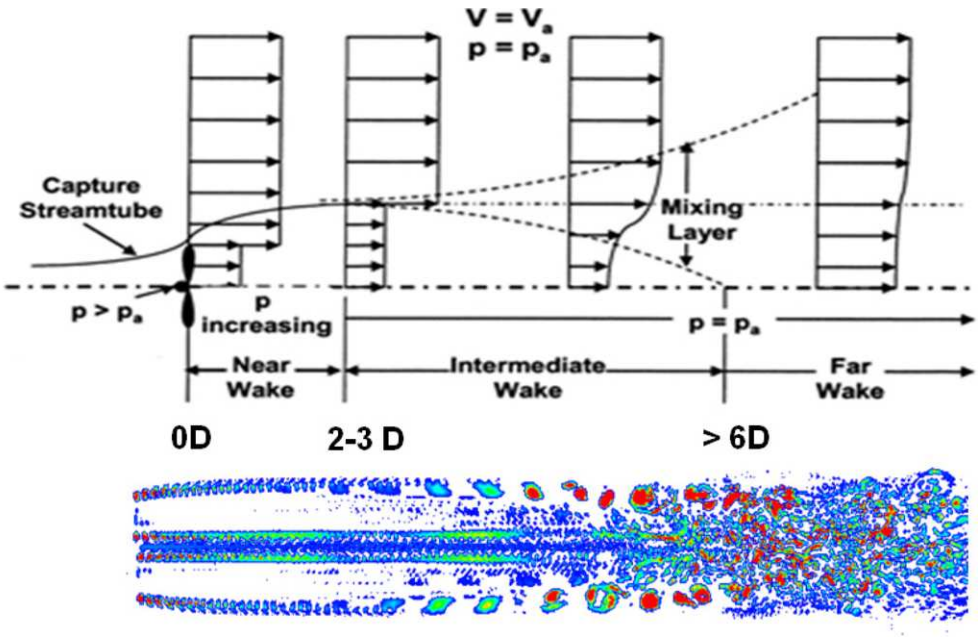

Figure 2.1.3: Near and far wake in a wind turbine (figure obtained from Jha et al., 2015)

2.1.2 Far wakes

The far wake effects focus mainly on the combined influence of the wakes from individual wind turbines when placed in wind farms. The total far wake effects might result from a single wind farm or a cluster of wind farms that are located closely together and might affect a large area surrounding the area of interest.
In this region, the bundled tip vortex structures break down into progressively finer scales of inhomogeneous turbulence. After this process is completed, the wake can be considered as fully developed, and the recovery of the wake momentum deficit continues.
Another type of numerical models than those mentioned in the previous section are required to solve these phenomena. In these cases, the area of interest is generally to big to be simulated with a standard microscale model. The WRF model provides an alternative to this constraint since it works with lower resolutions and less computational power, but at the same time includes real turbine information.

2.1.3 Wake models

There are several commercial and open source models based on multiple methodologies, being it empirical/analytical or based on CFD . Some of the most widely used commercial wind resource assessment tools like WAsP[2], Windsim[3], Windographer[4] include several methods to calculate wind turbine wakes.
Some of the most common models are the Jensen model (Jensen, 1983), which is one of the

[2] http://www.wasp.dk/
[3] https://www.windsim.com
[4] https://www.windographer.com

most simple and widely used, the Frandsen model (Frandsen, 2006) which is similar to the Jensen model and the semi analytical model developed by Larsen, 1983.
Other models, more complex, like the CFDWake model (Cabezón et al., 2009), developed at the CENER[5] are also used. This model is an elliptic CFD wind farm model which allows the simulation of wake effects inside big wind farms through the actuator disk[6] concept.
All the models mentioned are usually applied to the simulation of near wakes, providing a static wind speed deficit that depends on wind direction, position and type of wind turbines.
Lately, mesoscale models are being used to simulate the far wake effects of single or cluster of wind farms. These models don't require as much computational power than the standard microscale models and provide time varying results that can be very useful in the analysis of the region of interest.

2.1.3.1 WRF WIND FARM PARAMETERIZATION

Since version 3.3, the WRF model includes a wind farm parameterization (Fitch et al., 2012). This parameterization uses real wind turbines positions and characteristics and can be activated in the WRF configuration. It has advantages and disadvantages regarding other wake models like the possibility to obtain a time varying result instead of a static output, but it cannot properly simulate individual wind turbine wakes due to the low resolution of the mesoscale models.
The typical domain resolution in mesoscale models is lower than the distance between two consecutive wind turbines inside a wind farm. In some cases it originates that more than one wind turbine are contained in the same given grid cell. When that happens, the model provides the total wind deficit generated by all the wind turbines inside that computational cell, not being possible to distinguish between the individual wakes.
One might think that increasing the domain resolution would allow to overcome that constraint, but accordingly to the paper from Ito et al., 2015, the horizontal resolution of the mesocale domain should not be higher than 1km. At higher resolutions, the model attempts to resolve the turbulent eddies, but the Planetary Boundary Layer (PBL) parameterization assumes that all the turbulence is unresolved, creating inconsistencies in the results.
Another reason why the resolution should not be higher than 1km is that the parameterizations is designed to simulate the far-wake flow of wind turbines. Fitch, 2015 proposes a maximum horizontal resolution of the domain around 5 rotor diameters. This distance is usually interpreted as the separation between near and far wakes regions. Since the parameterization does not take into account the rotation of the blades, important in the near wake region, it is recommended to use it to simulate far wake effects.
An advantage of this approach is the possibility of simulating the atmosphere as a 4D environment (x, y, z, t) as opposed to the other stationary wake models mentioned in the previous sections. Using the WRF model enables the user to simulate the temporal evolution of the wake, making it possible to observe the wake meandering, increase or decrease of

[5] http://www.cener.com
[6] the forces are distributed over the entire rotor area

intensity, depending on the wind conditions calculated by the mesoscale model.
The typical microscale wake models are usually forced by an average inflow velocity and return a static output. The mesoscale model parameterization uses the instantaneous WRF wind speed as forcing, generating a time dependent output that adjusts itself to the wind conditions in the entire domain. Wake meandering and perturbations due to different wind speeds and direction in the wake path are taken into account, generating more realistic outputs.
This parameterization assumes that from the total Kinetic Energy (KE) extracted from the atmosphere, a fraction is converted to electrical energy while other fraction is consumed by electrical and mechanical losses, as well as nonproductive drag.
The force of drag induced by a wind turbine on the air flow can be calculated using the equation 2.1.1.

$$\mathbf{F}_{Drag} = \frac{1}{2} C_t(|\mathbf{V}|)\rho\,|\mathbf{V}|\,\mathbf{V}A \tag{2.1.1}$$

where $\mathbf{V} = (u, v)$ is the horizontal velocity vector (assumed uniform over the rotor area), C_t is the turbine thrust coefficient (assumed independent of air density), ρ is the air density, and $A = \left(\frac{\pi}{4}\right) D^2$ is the cross-sectional rotor area, being D the diameter of the turbine blades. Assuming that the turbines are always perpendicular to the flow and since the vertical profile of the horizontal wind is generally nonuniform, the rate of loss of KE from the atmosphere due to one wind turbine, integrated over the rotor area, is given by equation 2.1.2.

$$\frac{\partial KE_{drag}}{\partial t} = -\frac{1}{2}\int_{A_R} C_t(|\mathbf{V}|)\rho\,|\mathbf{V}|^3\,dA \tag{2.1.2}$$

The horizontal resolution of the innermost WRF domain used in this configuration is 3km. This grid spacing is bigger than the separation between consecutive wind turbines inside the wind farm. As mentioned before, this constraint implies that several wind turbines are placed inside the same grid cell. To accommodate for this situation, a density of wind turbines, $N_t^{i,j}$, is defined where i and j are the indices of the model grid cell in the the zonal and meridional directions. The rate loss of KE in a grid cell, written in terms of the grid indices i, j and k, corresponding to the cartesians coordinates x, y and z, is shown in equation 2.1.3.

$$\frac{\partial KE_{drag}^{i,j,k}}{\partial t} = -\frac{1}{2}\Delta x\Delta y N_t^{i,j} C_t(\left|\mathbf{V}_{i,j,k}\right|)\rho_{i,j,k}\,|\mathbf{V}|_{i,j,k}^3\,A_{i,j,k} \tag{2.1.3}$$

where $A_{i,j,k}$ is the cross-sectional rotor area of one wind turbine delimited by model levels k, $k+1$ in the grid cell i, j. This approach only accounts for wake effects between consecutive grid cells and not between turbines located in the same cell.
The KE loss due to wind turbines in one grid cell, is taken from the total KE in that grid cell. The total rate of change in one grid cell i, j, k is given by 2.1.4.

$$\frac{\partial KE_{cell}^{i,j,k}}{\partial t} = \frac{\partial}{\partial t}\int_{\Delta x}\int_{\Delta y}\int_{\Delta z} \frac{\rho_{i,j,k}}{2}(u_{i,j,k}^2 + v_{i,j,k}^2 + w_{i,j,k}^2)\,dz\,dy\,dx \tag{2.1.4}$$

where $\Delta z = z_{k+1} - z_k$, and z_k is the height at model level k. Assuming that only the horizontal wind component is affected by the wind turbine drag, we obtain equation 2.1.6.

$$\frac{\partial KE_{cell}^{i,j,k}}{\partial t} = \frac{\partial}{\partial t}\frac{\rho_{i,j,k}|\mathbf{V}|^2}{2}(z_{k+1} - z_k)\Delta x \Delta y \tag{2.1.5}$$

$$= \rho_{i,j,k}|\mathbf{V}|_{i,j,k}\frac{\partial |\mathbf{V}|_{i,j,k}}{\partial t}(z_{k+1} - z_k)\Delta x \Delta y \tag{2.1.6}$$

Within a grid cell i,j,k the rate of change of KE is equal to the rate of loss of KE due to the wind turbines in that cell. From equations 2.1.3 and 2.1.6 it is possible to obtain the momentum tendency term given by equation 2.1.7.

$$\frac{\partial |\mathbf{V}|_{i,j,k}}{\partial t} = -\frac{\frac{1}{2}N_t^{i,j}C_T(|\mathbf{V}|_{i,j,k})|\mathbf{V}|_{i,j,k}^2 A_{i,j,k}}{(z_{k+1} - z_k)} \tag{2.1.7}$$

Expressing equation 2.1.7 in component form, giving the horizontal momentum tendency terms, that can be applied in the model:

$$\begin{cases} \frac{\partial u_{i,j,k}}{\partial t} = \frac{u_{i,j,k}}{|\mathbf{V}|_{i,j,k}}\frac{\partial |\mathbf{V}|_{i,j,k}}{\partial t} \\ \frac{\partial v_{i,j,k}}{\partial t} = \frac{v_{i,j,k}}{|\mathbf{V}|_{i,j,k}}\frac{\partial |\mathbf{V}|_{i,j,k}}{\partial t} \end{cases} \tag{2.1.8}$$

The power extracted by the wind turbines which is converted to electrical energy is thus given by equation 2.1.9.

$$\frac{\partial P_{ijk}}{\partial t} = \frac{\frac{1}{2}N_t^{i,j}C_P(|\mathbf{V}_{i,j,k}|)|\mathbf{V}|_{i,j,k}^3 A_{i,j,k}}{(z_{k+1} - z_k)} \tag{2.1.9}$$

where $z_{k+1} - z_k = \Delta z$, being z_k the height at model level k and C_P the power coefficient.
The fraction of KE that is not converted into electricity is converted into Turbulent Kinetic Energy (TKE) and it is given by equation 2.1.10.

$$\frac{\partial TKE_{ijk}}{\partial t} = \frac{\frac{1}{2}N_t^{i,j}C_{TKE}(|\mathbf{V}_{ijk}|)|\mathbf{V}|_{ijk}^3 A_{ijk}}{(z_{k+1} - z_k)} \tag{2.1.10}$$

Real wind turbine characteristics along with real turbine positions are used in the wake simulations.
The EERA-DTOC project, mentioned on section 1.1, conducted several test-cases in order to explore the capabilities of the recently developed wind farm parameterizations included in the WRF model. Pre-selected SAR (Christiansen and Hasager, 2005) satellite images with visible wakes generated by several wind farms were compared to mesoscale model outputs from different companies participating in the project. Due to lack of available measurements and the uncertainties in the SAR wind speeds, only the shape, meandering and extension of the simulated far wakes were analysed (Hasager et al., 2015). All the results seemed to indicate that the mesoscale model was able to emulate most of the wakes observed in the SAR images. Figure 2.1.4 shows some example of far wakes obtained with the WRF model, using CENER's

methodology in the Alpha Ventus[7] and Egmond aan Zee[8] wind farms. Both examples indicate that the Fitch (Fitch et al., 2012) wind farm parameterization is able to reproduce the shape, length and direction of the observed wakes, despite that some of the SAR images are not very clear. The study also concluded that if the wind conditions were similar, far wakes would extend over a larger area in very stable and neutral atmospheric stability while in very unstable conditions the wind speed recovered faster.

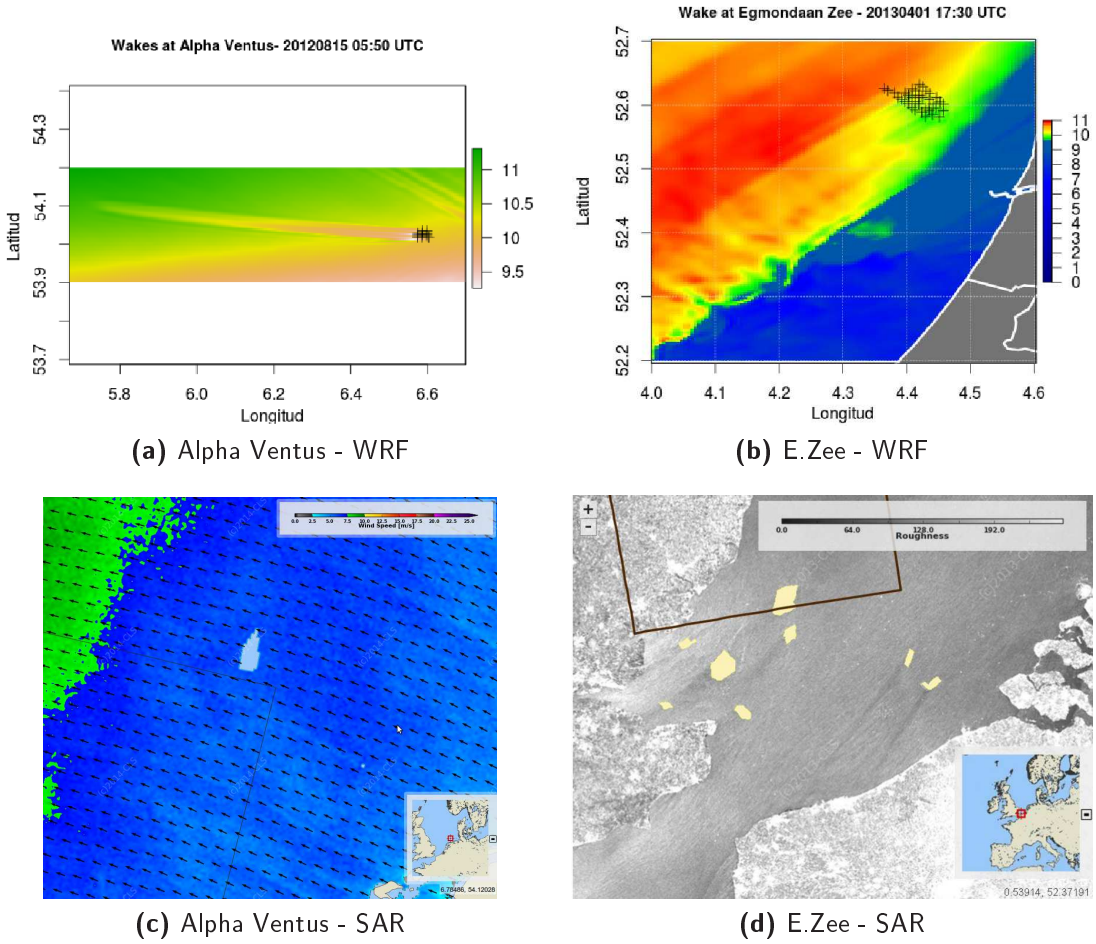

(a) Alpha Ventus - WRF

(b) E.Zee - WRF

(c) Alpha Ventus - SAR

(d) E.Zee - SAR

Figure 2.1.4: Comparison between the WRF simulations in a specific instant in the Alpha Ventus (a) and Egmond aan Zee (b) wind farms and the SAR images (c) and (d). The simulations were performed by CENER, using the version 3.6 of the WRF model and its wind farm parameterization (Hasager et al., 2015). The domain and methodology used are similar to the one described in this work.

[7] http://www.4coffshore.com/windfarms/alpha-ventus-germany-de01.html
[8] http://www.4coffshore.com/windfarms/egmond-aan-zee-netherlands-nl02.html

CHAPTER 3

METHODOLOGY

The final goal of the EERA-DTOC project, mentioned on section 1.1 was to create a commercial tool capable of performing multiple studies regarding all the stages of the construction and operation of an offshore wind farm. Wind climate conditions, wind farm layout generation, minimizing the losses due to far and near wake effects and optimizing the distance to the electrical grid and power stations, economical modelling and risk management are tasks performed by the final developed application[1]. Several companies are connected to this tool and when a given user asks for a determined study, the application automatically sends all the required information to the company that will perform the task. That task is then automatically executed in that company facilities and the results are sent back to the client through the application. Since the companies involved in this collaboration have different computational capabilities, a set of minimum requirements was defined in order to provide the user a response in a commercially adequate deadline but still with enough "quality" to fulfil the client's needs. From the mesoscale models point of view, these requirements included a minimum horizontal resolution, number of vertical levels, minimum domain size, minimum period to simulate and a maximum deadline to deliver the post-processed results to the client.

At CENER, with the current computational capabilities it was very difficult to perform a 10 years (minimum defined in the requirements) mesoscale simulation in less than two weeks (deadline also defined in the requirements). In order to overcome this problem and still be part of this collaboration, a methodology capable of create a typical year, representative of the long term period was developed. The typical year methodology, combined with the use of the WRF wind farm parameterization and configurations presented in the following sections, allowed CENER to achieve the requirements defined by the EERA-DTOC commercial tool and to create a "low cost" alternative that is capable of simulating the far wake effects on offshore wind farms provoked by other neighbouring wind farms.

In the next sections, it is included a description of the methodology used to obtain the meteorological typical year, the WRF model configuration and all the numerical simulations

[1] http://www.wind-and-economy.com/home/

performed.

3.1 METEOROLOGICAL TYPICAL YEAR[2]

The numerical experiments will be performed using boundary conditions that are representative of the meteorological conditions observed in a large region including the domain to be simulated. For that purpose, we construct a typical year of synoptic conditions, defined by its optimal similarity with the long-term characteristics of a selected variable used as a proxy of the wind climate.

A Monte Carlo method with stratified sampling is used to generate around 100000 combinations of candidate periods which are then compared to the long-term period.

The daily average Mean Sea-Level Pressure (MSLP) from the Modern-Era Retrospective Analysis for Research and Applications (MERRA)[3] reanalysis database, for each day in every typical-year combination is represented and image processing techniques are used to identify a synthetic reference period whose maps of the average MSLP and its standard deviation best match the corresponding long-term maps. The MERRA data was chosen instead of other sources of information due to its high horizontal resolution (0.5 degrees in latitude and 0.67 degrees on longitude) and the 1 hour output frequency of the 2D meteorological variables.

Four different image processing techniques are used to evaluate image similarity for both mean and standard deviation MSLP maps which are then averaged into one image similarity error index after applying a linear normalization operator to each sub-index. An optimal or representative set of days is selected by requiring the error index to be minimal (Chavez-Arroyo et al., 2015).

In order to eliminate seasonal tendencies, the typical year will be composed of 365 days in which the first day will be the most representative January first, the second day will be the most representative January second and following the same logic, the last day is the most representative December thirty-first from the entire wind climate period. This way it is ensured that the final typical year does not present seasonal meteorological deviations due to an irregular distribution of dates throughout the chosen period.

Several evaluation techniques of this methodology were used to determine the optimal approach, following the scheme presented in 3.1.1. Methods based on Principal Component Analysis (PCA), a non-linear technique named Self-Organizing Maps (SOM) (Kohonen, 1995), a traditional industry method (TRAD) based on a purely random selection of 365 days, as well as a novel approach termed Best Annual Mean and Standard Deviation (BAMS) were tested. The four proposed methods share the same goal and although they share the same common Monte Carlo principle, they address the problem of climate similitude with different tools and alternative perspectives.

[2] This section is a brief resume extracted by the PhD thesis from Dr. Roberto Chavez (Chavez-Arroyo, 2014) that attempts to give a brief explanation to the methodology used in the meteorological typical year calculation used in this dissertation.

[3] global reanalysis project that was undertaken by the NASA Global Modelling and Association Office (GMAO) http://gmao.gsfc.nasa.gov/merra/

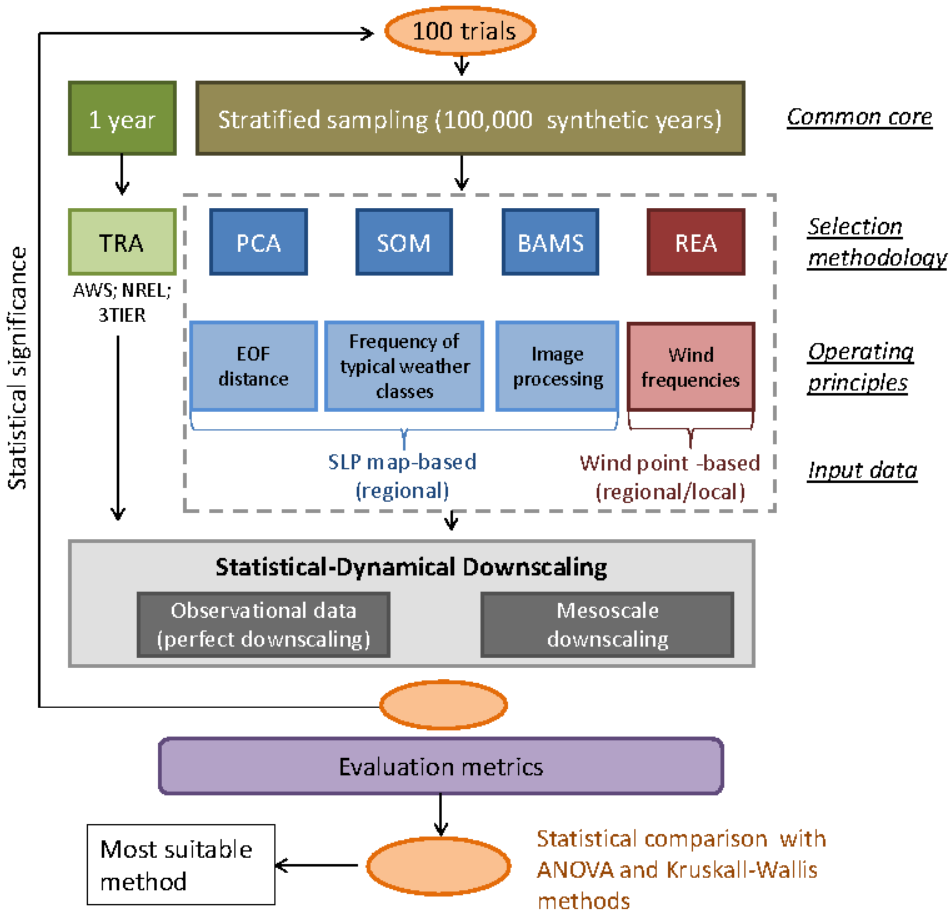

Figure 3.1.1: Schematic of the overall typical year methodology work flow proposed in the thesis from Chavez-Arroyo, 2014

The methods have been tested both on a network of automatic surface observation stations in the Spanish region of Navarra and long-term downscaled wind resource maps were created for the Iberian peninsula with the mesoscale model SKIRON (Kallos et al., 2005). Extensive statistical tests for group comparisons, both parametric (Analysis of variance (ANOVA)) and non-parametric (*Kruskall Wallis*), were conducted on the data sets and showed a distinctive performance of the methods (see Chavez-Arroyo, 2014 for more details).
The results from Chavez-Arroyo, 2014 showed that the BAMS method was the most solid among all tested and the one which obtained the better correlation between the large and representative periods. In section 3.1.1 a description of this approach is presented in more detail.

3.1.1 BAMS

The BAMS method is based on two key elements. The first one is the use of MSLP mesoscale maps for a region as predictors and the second is the use of stratified sampling techniques based on the work from Rife et al., 2013. The novel approach in the BAMS method regards how

the similarity between the long-term and representative period is established. This method uses a mesoscale approach in an attempt to obtain a metric capable of indicate the level of similarity between two images. This metric, combines four different image similarity detection techniques into one single indicator capable of determine the performance of the method.

The first image similarity technique consists in the Root Mean Square Error (RMSE) calculation of the point to point comparison between the long-term and representative period MSLP maps. The second refers to an average Pearson correlation coefficient between rows and columns from each pair of maps, the third technique directly compares the values of the MSLP contained in each row and column of both images, and finally, the last comparison is based on a structural similarity index proposed by Wang et al., 2004 that tries to quantify the visibility of the errors between a distorted and a reference image.

Basically, all the four techniques are trying to determine the similarity between two figures that illustrate the MSLP in the North-Atlantic region. To the human eye, it is relatively simple to do so, but to translate this capability to an algorithm is a very complex issue. The first technique uses the point by point MSLP real values from each figure and calculates the RMSE between the two obtained data sets. The problem with this methodology arises when the governing synoptic patterns in two images, very similar for the human eye (figure 3.1.2), are slightly displaced, translating to a very high RMSE, which is an indicator of low similarity. To overcome this problem, the other three techniques are used to balance the final metric. Comparisons between the position of the center and size of the governing synoptic patterns in each image are made along with analysis between the MSLP values in entire rows and columns, in order to capture the horizontal and vertical displacement as well as the average MSLP of each governing synoptic pattern. Combining all four methods makes possible to identify in a very satisfactory way which MSLP patterns from the generated candidates are the most similar to the long term period and consequently, obtain the set of dates that will constitute the optimal typical year.

Figure 3.1.3 shows the absolute wind speed error in the Iberian Peninsula, using the SKIRON mesoscale model and applying this method.

It is possible to see that almost the entire peninsula has a very low wind speed error, with the exception of a small area near the Mediterranean Sea which seems to concur with the Spanish region of Valencia. For the other regions, the values seems to be almost homogeneous and no significant differences in errors were noticed between different types of terrain orography or geographical characteristics, which is a good sign regarding this method robustness.

Concerning the energy density error, the exact situation is verified, but given the cubic dependence of the wind energy in the wind speed, the error is slightly higher.

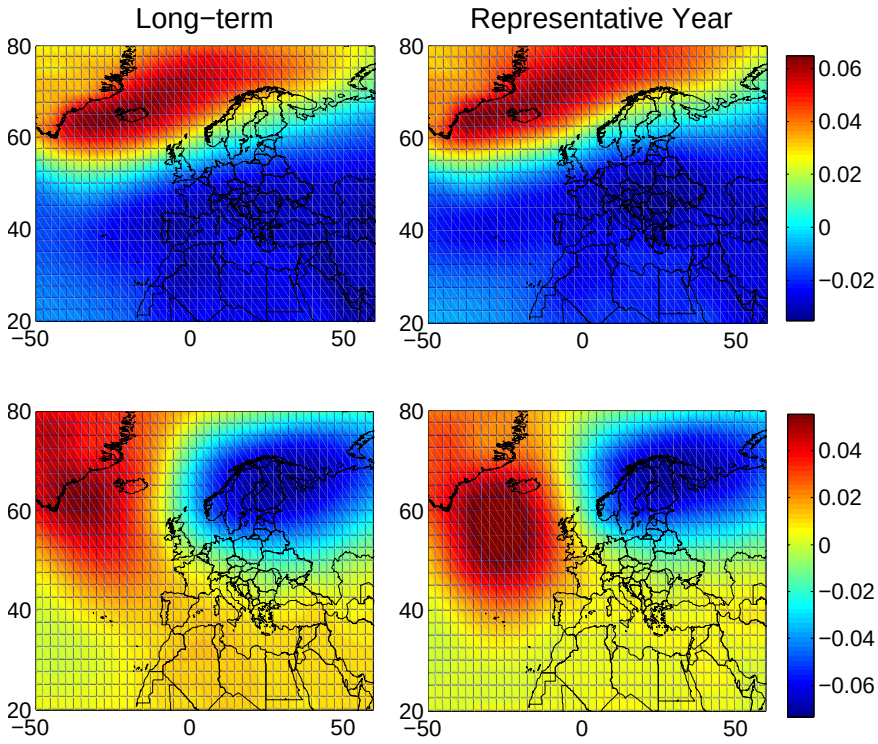

Figure 3.1.2: Representation of the first (above) and second (bellow) Empirical Orthogonal Functions (EOF) from the long term period MSLP (left) and two candidate periods (right). To the human eye it is possible to see a high similarity between the typical year candidates and the long term period in both cases, but it is not easy to translate that comparison to an algorithm, (Chavez-Arroyo, 2014).

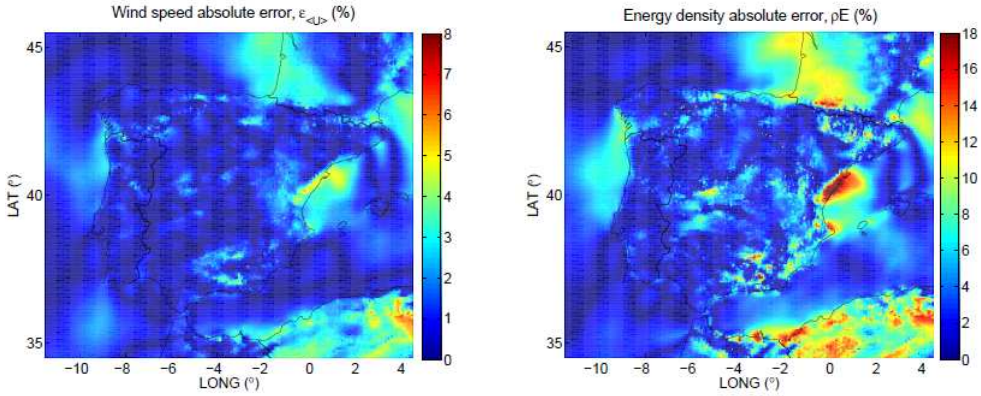

(a) Wind speed **(b)** Energy Density

Figure 3.1.3: Absolute wind speed error and absolute energy density error of one realization of the BAMS method (Chavez-Arroyo, 2014).

3.1.2 Meteorological Typical Year: Results and Conclusions

All methods mentioned before were compared with the numerical model SKIRON simulations. PCA, SOM, BAMS, the Rife method in its REA1[4] and REA2[5] implementations and finally, the

[4]The Rife method requires data from a Reanalysis location. Only one point from the seven reanalysis points located in Navarra was chosen to perform the comparison with the 22 weather stations. REA1 represents the point with the highest average correlation amongst all stations.

traditional industry method were compared with the SKIRON wind speed results at 80m a.g.l., since the main goal is to obtain a robust statistical-dynamical downscaling methodology that allows to reduce the computational effort required to perform a long-term simulation of a large area.

Two metrics were defined in order to provide a clear understanding of the capability of each method:

$$\varepsilon_x = \left| \frac{x^{LT} - x^{RP}}{x^{LT}} \right| \times 100\,[\%] \tag{3.1.1}$$

$$D = \sum_{g=1}^{nbins} w_g \left| \frac{f_g^{LT} - f_g^{RP}}{f_g^{LT}} \right| \times 100\,[\%] \tag{3.1.2}$$

The first metric is the Relative Absolute Error (RAE) between the long-term wind speed, x^{LT}, and the representative period wind speed, x^{RP}. The second metric is relative to the wind speed frequency difference, where f_g^{LT} and f_g^{RP} are the relative wind speed frequencies corresponding to the long-term and representative periods and w_g is a weighting factor taken from the long-term frequency that assigns more importance to the bins with higher frequency of occurrence.

In figure 3.1.4 the global error in the wind speed prediction, $\varepsilon_{<U>}$, and the metric measuring the wind speed probability distributions, D, are illustrated.

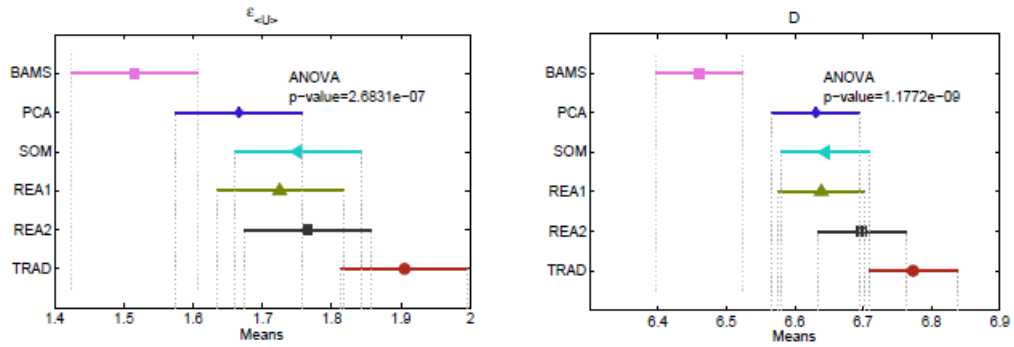

(a) $\varepsilon_{<U>}$ **(b)** D

Figure 3.1.4: Average absolute error in the wind speed predictions and the metric representing the wind speed probability density for all the analysed methods (Chavez-Arroyo, 2014).

Both figures clearly shows that the BAMS technique outperforms every other method. The traditional method seems to produce the highest errors, while the SOM, PCA and Rife methods produce similar results. Based on all the results and validations performed, the BAMS method was chosen to generate the meteorological typical year, later simulated with the WRF model.

The typical year used in this study is calculated used the BAMS method, obtained from a 10 years period between 2001 and 2011. This period was chosen because it included the period in which all the measurements used in this study are available.

[5] REA2 represents the reanalysis point with the lowest average correlation in all 22 weather stations

3.2 NUMERICAL SIMULATIONS

Using the typical year methodology mentioned on section 3.1, 365 days from a 10 years period are chosen and generate a wind climate that is representative of the entire period. The typical year wind assessment should be equivalent to simulating the entire 10 years period, saving significant time and computational resources in the process.
For every chosen day, an independent WRF simulation is launched and the resulting outputs are used to reconstruct the typical year wind resource map. The mean wind resource assessment map from all the simulations is calculated by averaging the hourly wind records from the entire simulated period.
Three simulations are performed to cover all the scenarios at the HR wind farm. The scenarios refer to the period without any wind farms, when only the HR1 was built and finally the current scenario in which the HR2 is also operational.

- **Control:** No wind farms are considered and the wind farm parameterization is not activated. The obtained wind climate is used as the reference for the wind conditions in the region of interest.
- **Sim1:** Only the HR1 wind farm is considered. It calculates the theoretical impact of HR1 on HR2 and allows the validation of the methodology in the period "pre-construction" of the second wind farm.
- **Sim2:** Both HR1 and HR2 wind farms are computed into the domain. It calculates the current far wake effects on the surrounding area and allows the validation of the period "post-construction" of HR2 . It determines the influence of the HR2 wind farm on the "pre-existent" HR1 wind farm.

The first simulation pretends to calculate the far wake effects produced by the HR1 wind farm in the HR2 location and determine how much influence it has in the wind speed conditions at the HR2 wind farm. This configuration is also used to validate the WRF wind farm parameterization in the period before the construction of the HR2 .
The second configuration makes possible to determine the impact on the mean wind speed and power production at the HR1 wind farm, resulting from the construction of the second wind farm. Since there are no measurements available for the HR2 wind farm neither for the period after 2009, some assumptions have to be made in order to reach meaningful conclusions regarding the methodology.
At the HR wind farm site, there are three meteorological masts that were installed at different periods, with different purposes. The first mast (M2) was the first to be installed and was used to measure "in situ" the wind conditions at the HR1 location. Later, two more masts (M6 and M7) were installed "behind" the HR1 wind farm in order to measure the wind speed deficits due to the far wake effects.
The control run will be validated against the measurements from the mast M2 that was operational before the construction of both wind farms. These results will constitute the

validation of the simulated WRF "unperturbed" wind conditions.
The wind speeds from the Sim1 are compared with the measurements from the M6 and M7 masts and will determine the error of the wind farm parameterization methodology predictions. The wind speeds from the same simulation are converted to wind power using the power curve of each wind turbine and validated against the measured wind power dataset for the HR1 wind farm that was provided by Kurt Hansen. That way, it is possible to determine the error associated to the wind farm parameterization simulations.
The Sim2 will be used to ascertain the wind speed deficit at the HR1 wind farm after the construction of the second wind farm. The mean wind power production of the HR1 wind farm is calculated for both cases, the data is synchronized in order to have the same period and number of records and the difference between the power productions of the two simulations will reflect how much the construction of the HR2 wind farm has affected the HR1 wind farm production.

3.3 WRF Domain configuration

WRF version 3.6 (Skamarock et al., 2008) is used. Three, two-way nested domains are configured with resolutions of 27, 9 and 3km resolutions and 35 vertical levels from the surface until the top of the atmosphere, located at 25mbar. The uneven vertical distribution of the model levels assures a higher concentration of levels near the surface, which results in a higher vertical resolution near the surface, allowing a properly simulation of the complexities of the PBL . All three domains are centred at 55.25°N; 7.5°E and are constituted by 110x110, 100x100 and 88x88 points respectively.
ERA-Interim reanalysis (Dee, 2011) is used as boundary conditions to the WRF model and the wind farm parameterization is activated in the innermost domain. Table 3.3.1 describes every parameterization used in the simulation.

Parameterization	Scheme
Microphysics	WRF Single-Moment (WSM) (Hong et al., 2004)
Long wave radiation	Rapid Radiative Transfer Model (Mlawer et al., 1997)
Shortwave radiation	Dudhia scheme (Dudhia, 1989)
Surface layer	Mellor-Yamada-Nakanishi-Niino (MYNN) (Nakanishi and Niino, 2004)
Land surface	Noah (Chen and Dudhia, 2001)
Planetary Boundary Layer	MYNN 2.5 level TKE scheme (Nakanishi and Niino, 2004)
Cumulus	Kain-Fritsch (new Eta) (Kain and Fritsch, 1990)

Table 3.3.1: Parameterizations schemes used

Should be mentioned that the wind farm parameterization is only compatible with the MYNN PBL parameterization, which somehow limits the array of available parameterization choices.
Real turbine positions, turbine power and thrust coefficient curves, turbine radius and real hub heights are used to emulate the wind farm characteristics.
In order to cover the entire typical year period calculated by the methodology mentioned in

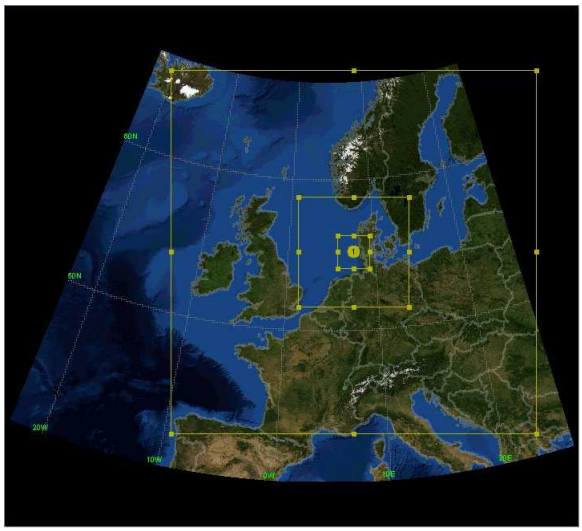

Figure 3.3.1: Domain configuration for the Horns Rev test case

section 3.1, 365 independent simulations were made. Each run has an horizon of 30 hours where the the first 6 hours of simulation are discarded. Based on the acquired experience using the WRF model both applied to daily operational forecast and wind resource assessment in multiple locations around the globe, it is assumed that after the initial 6 hours, the model has fully spin-up[6] and the results are valid.

[6]The time the model takes to reach an equilibrium state.

CHAPTER 4

TEST CASE DESCRIPTION

4.1 HORNS REV WIND FARM

The HR wind farm is located approximately at 15km from the coast of Denmark (55°31'47"N 7°54'22"E) and it is composed by two operating wind farms, HR1 and HR2 (figure 4.1.1). HR1 built in 2002, was the first operating large scale offshore wind farm in the world and has an installed capacity of 120MW. It is constituted by 80 wind turbines from *Vestas* (V80 - 2MW ; figure 4.2.1) that are arranged in a regular array of 5km x 3.8km formed by 10 columns and 8 rows. The internal spacing between the turbines is 7D[1] along the East-West direction with spacing of 9.4D or 10.4D along the diagonals. Aerial photos of both wind farms can be seen on figure 4.1.2.
The HR2 wind farm was inaugurated in 2009, also becoming the biggest offshore wind farm in world at that time. It is located North of the HR1 wind farm (55°36'00"N 7°35'24"E) and it is constituted by 91 *Siemens Wind Power* SWP 2.3-93 wind turbines (figure 4.2.2) with a total generating capacity of 209 MW. The position and brand for each individual wind turbine are presented in tables A.0.1 and A.0.2.

4.2 WIND TURBINES

Two types of wind turbines were installed in the HR1 and HR2 wind farms. The Vestas V80-2MW[2] is used in the HR1 and the Siemens SWT-2.3MW-93[3] is used in the HR2 wind farm.

4.2.1 VESTAS WIND TURBINE

This wind turbine was developed by Vestas and has a Rated Power of 2MW. It has a diameter of 80m, the cut in[4] and cut out[5] wind speeds are 4m/s and 25m/s respectively and the hub height

[1] **7D** refers to seven wind turbine diameters. It is a common notation when working with microscale wake models.
[2] http://www.4coffshore.com/windfarms/turbine-vestas-v80-2.0-mw–tid53.html
[3] http://www.4coffshore.com/windfarms/turbine-siemens-swt-2.3-93-tid41.html
[4] minimum wind speed at which the turbine blades overcome friction and begin to rotate
[5] wind speed at which the turbine blades are brought to rest to avoid damage from high winds

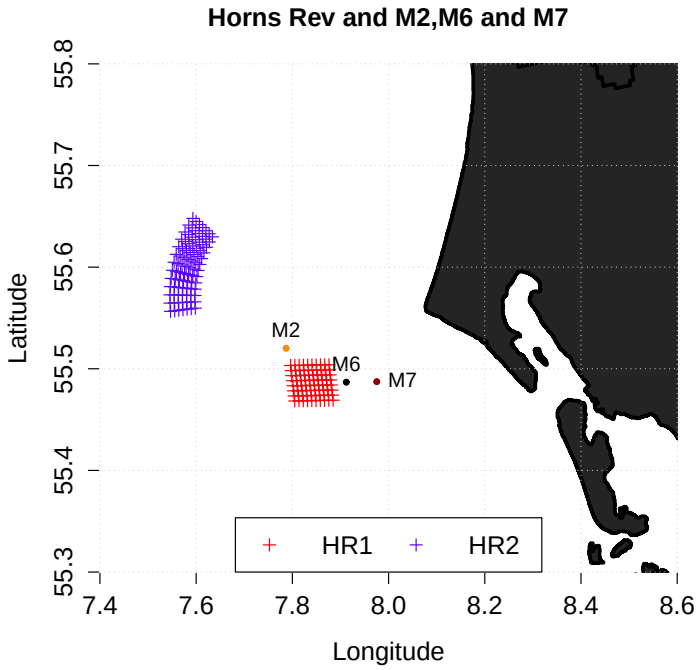

Figure 4.1.1: Locations of Horns Rev 1 (red), 2 (blue) and masts (M2, M6 and M7)

is 70m (figure 4.1.2(c)).
In figure 4.2.1 the power and thrust curves are represented.

4.2.2 Siemens wind turbine

This wind turbine was developed by Siemens and has a Rated Power of 2.3MW. It has a diameter of 93m, the cut in and cut out wind speeds are 4m/s and 5m/s respectively and the hub height is 70m (figure 4.1.2(d)).
In figure 4.2.2 the power and thrust curves are represented.

4.3 Measurements

4.3.1 Masts

Three masts are used to validate the methodology and their exact location is represented in figure 4.1.1. Mast M2(55.52013°N;7.786965°E), has a height of 62 m and was installed prior to the wind farm installation to record the wind conditions at the site. Later, two identical masts M6(55.48680°N;7.912065°E) and M7(55.48735°N;7.975354°E) were installed as part of the Horns Rev wind farm wake measurements program and have the same height as the wind turbines (70 m). Masts M6 and M7 are located 8.3km and 12.3km East of the HR1 wind farm and their instrumentation consists on high quality cup anemometers, vanes and thermometers for measuring wind speeds, wind directions and air and water temperatures. The instrumentation has been in operation since 2004 with annual calibration and

(a) HR1

(b) HR2

(c) V80-2MW

(d) SWT-2.3MW-93

Figure 4.1.2: Aerial photos of Horns Rev 1 and Horns Rev 2 (top) and pictures of the V80-2MW and SWT-2.3MW-93 wind turbines (bottom).

inspections.

Mast M2 measured 10 minutes wind speed and direction at 15, 30, 45 and 62m height a.s.l. from 1999 to 2004. Masts M6 and M7 measured 10 minutes wind speed and direction at 20, 30, 50, 60 and 80m height between 2005 and 2009.

All data has been filtered in order to eliminate wrong measurements and to correct the shadow effect from the mast tower. The 10 minutes records are averaged to hourly records to be comparable to the WRF simulations output. These measurements are later synchronized with the typical year dates and WRF outputs from all the simulations in order to perform the several required validations.

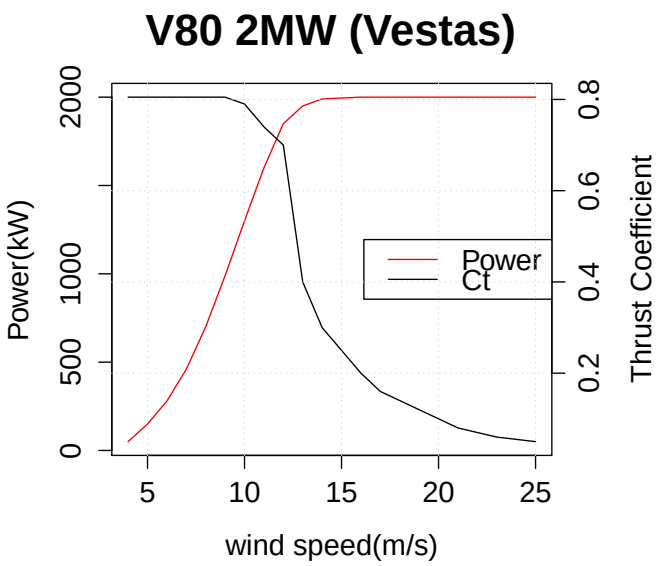

Wind speed	Ct	Power(kW)
4	0.805	50.0
5	0.805	150.0
6	0.805	280.0
7	0.805	460.0
8	0.805	700.0
9	0.805	990.0
10	0.790	1300.0
11	0.740	1600.0
12	0.700	1850.0
13	0.400	1950.0
14	0.300	1990.0
15	0.250	1995.0
16	0.200	2000.0
17	0.160	2000.0
18	0.140	2000.0
19	0.120	2000.0
20	0.100	2000.0
21	0.080	2000.0
22	0.070	2000.0
23	0.060	2000.0
24	0.055	2000.0
25	0.050	2000.0

Figure 4.2.1: Power and thrust curves for the V80-2MW turbine

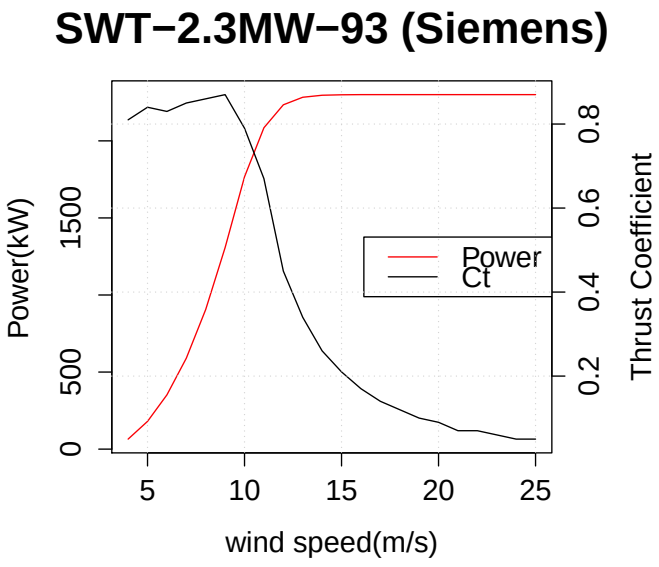

Wind speed	Ct	Power(kW)
4	0.81	65.0
5	0.84	180.0
6	0.83	352.0
7	0.85	590.0
8	0.86	906.0
9	0.87	1308.0
10	0.79	1767.0
11	0.67	2085.0
12	0.45	2234.0
13	0.34	2283.0
14	0.26	2296.0
15	0.21	2299.0
16	0.17	2300.0
17	0.14	2300.0
18	0.12	2300.0
19	0.1	2300.0
20	0.09	2300.0
21	0.07	2300.0
22	0.07	2300.0
23	0.06	2300.0
24	0.05	2300.0
25	0.05	2300.0

Figure 4.2.2: Power and thrust curves for the SWT-2.3MW-93 turbine

4.3.2 WIND TURBINE POWER PRODUCTION

A database of Horns Rev wind farm has been compiled by Kurt S. Hansen from DTU to support many studies on offshore wake effects. It comprises a period of 5 years, from January 2005 to December 2009, of 10-min registers. The database includes the power output from every individual wind turbine along with its velocity and wind direction at hub height. The

power production has a quality "flag" that indicates whether the measurements are reliable or if they are "perturbed"[6]. Only the data with the quality flag equal to "valid" was used in the validations while all the other records were ignored.
Using this database is convenient to adopt the same quality-check filtering that has been done on the data in previous studies from DTU (Hansen et al., 2010 and Hansen, 2011). This consistency is important in order to avoid user-dependencies in this filtering process which can result in important discrepancies.

[6]These perturbations might refer to incorrect measurements, power regulation from the control center, start and stop sequence of the machine, etc

CHAPTER 5

RESULTS AND VALIDATIONS

The results from all three simulations are presented in this chapter. In section 5.1 the average wind map from the control run and the two different wind farm configurations are shown. Using the available measurements from the M2, M6 and M7 masts, the wind resource map and the wind farm parameterization are validated. The error metrics Bias, Mean Absolute Error (MAE) , RMSE , R^2 and the error percentage are calculated as described by equations 5.0.1 to 5.0.5.

$$Bias = \frac{1}{N}\sum_{i=1}^{N}[W_{sim.}(i) - W_{meas.}(i)] \tag{5.0.1}$$

$$MAE = \frac{1}{N}\sum_{i=1}^{N}|W_{sim.}(i) - W_{meas.}(i)| \tag{5.0.2}$$

$$RMSE = \sqrt{\frac{1}{N}\sum_{i=1}^{N}|W_{sim.}(i) - W_{meas.}(i)|^2} \tag{5.0.3}$$

$$R^2 = 1 - \frac{\sum_{i=1}^{N}[W_{meas.}(i) - W_{sim.}(i)]^2}{\sum_{i=1}^{N}\left[W_{meas.}(i) - \overline{W_{sim.}(i)}\right]^2} \tag{5.0.4}$$

$$Error = \frac{1}{N}\sum_{i=1}^{N}\left[\frac{W_{sim.}(i) - W_{meas.}(i)}{W_{meas.}(i)}\right] * 100 \tag{5.0.5}$$

where $W_{sim.}$ refers to the simulated wind speed and $W_{meas.}$ refers to the measured wind speed.

The validations performed in each section refer to different periods that depend on the available measurements, stages of the HR construction and the type of analysis to be performed:

- **Wind climate:** The wind climate from the control run is validated in the 2001 to 2004 period, which corresponds to the available measurements period at the M2 mast. The

typical year dates which are comprehended in this period are selected and synchronized with the measurements from the M2 mast and the errors, described before, are calculated. It pretends to illustrate the robustness of the wind climate simulated with the WRF model.

- **WRF parameterization:** The parameterization is validated in the period between 2005 and 2009, corresponding to the available measurements in the M6 and M7 masts. Like the previous analysis, only the dates from the typical year comprehended in this period are used and synchronized with the measurements from both M6 and M7 masts. The errors calculated in this analysis try to ascertain the "quality" of the wind farm parametrization used.

- **Wind speed and Power deficit due to the far wake effects:** The wind speed and power deficits are calculated using the entire typical year, which is representative of the long term period.

5.1 WIND CLIMATE

The wind resource maps for the entire typical year at 70 and 80m for the control run and both WRF wind farm configurations are shown in figure 5.1.1. These maps are obtained by averaging all the wind speeds outputs at every grid point of the domain. The average wind speed obtained from the control run at the wind farm site is around 9 to 9.5 m/s at 70m and around 9.3 to 9.8 m/s at 80m.

Mast M2 provides measurements of the wind speed and direction at 15, 30, 45 and 62m a.s.l. from 2001 to 2004 that are used to validate the wind speed simulations in that same period. A good precision in the simulations is indispensable to obtain an accurate wind speed deficit estimation.

All records from the typical year covering the period between 2001 and 2004[1] (before the construction of the HR wind farm) are selected and synchronized with the measurements from the M2 mast. The wind speed from the 62m level are extrapolated to 70m using the wind profile power law (equation 5.1.1) and used to validate the wind climate at hub height.

$$u = u_r \left(\frac{Z}{Z_r} \right)^{\alpha} \tag{5.1.1}$$

where u is the wind speed, u_r is the reference wind speed, z is the height, z_r the reference height (62m) and α is an empirical coefficient derived from the atmospheric stability.

The α coefficient is calculated in every output time step, using the four available vertical levels time series. The resulting time series of α coefficients is averaged to a single mean value and used to extrapolate the wind speed from 62 to 70m.

Table 5.1.1 indicates the global error metrics of the control run when compared with the M2 mast measurements.

[1] This validation should only include the data from 2001 to 2002, as the HR1 wind farm was constructed in 2002. The slightly higher errors after 2003, seen in the monthly analysis figure are probably due to this error.

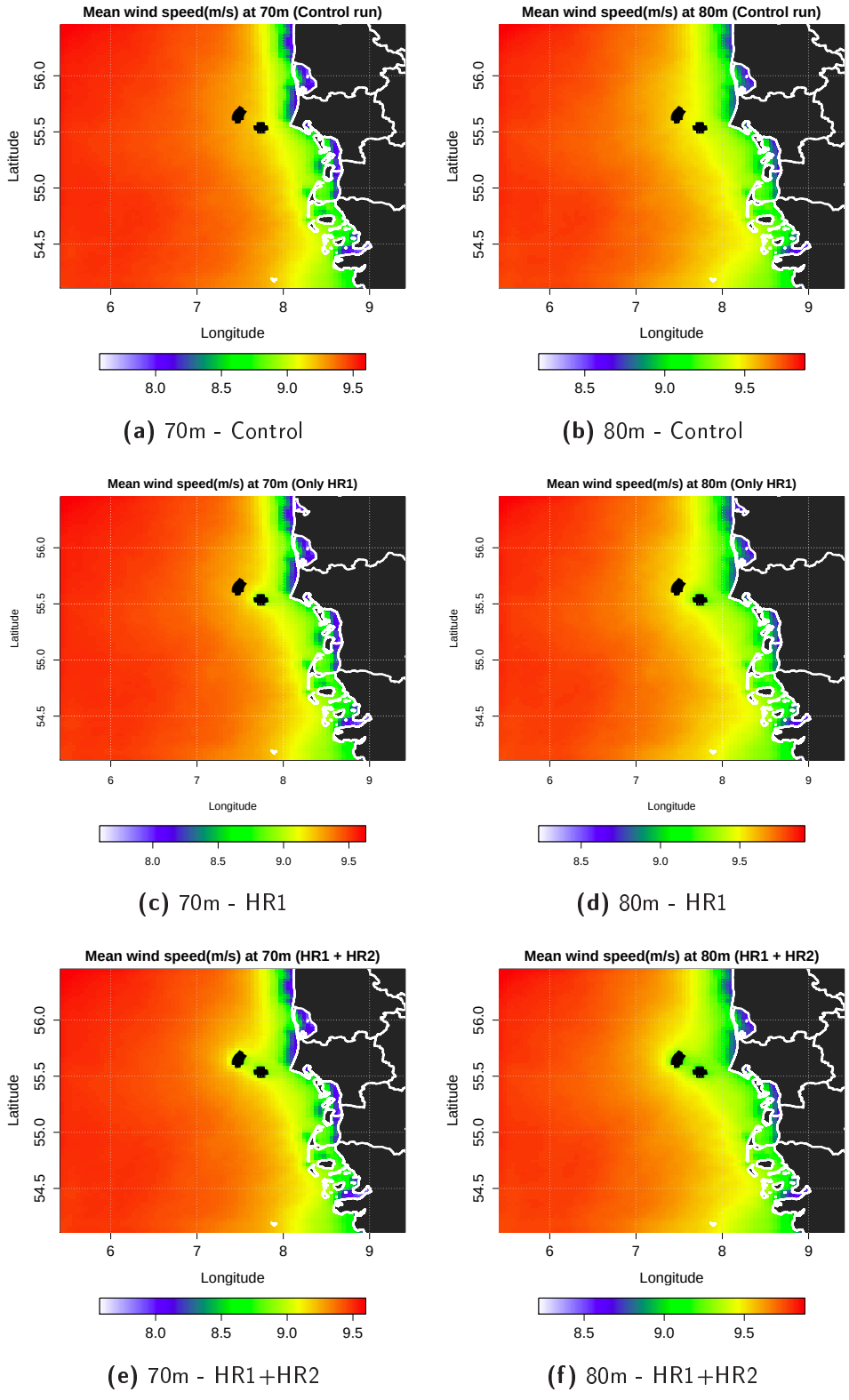

(a) 70m - Control

(b) 80m - Control

(c) 70m - HR1

(d) 80m - HR1

(e) 70m - HR1+HR2

(f) 80m - HR1+HR2

Figure 5.1.1: Mean wind speed(m/s) at 70m (left) and 80m (right)for the control run and both wake configurations for the typical year.

Bias	MAE	RMSE	R^2	Error(%)
0.38	1.44	1.94	0.83	4.19

Table 5.1.1: Global errors at 70m a.s.l. at the M2 mast location for the period between 2001 and 2004.

The relatively low Bias contributes to an error of 4.19%. A MAE of 1.44 m/s, a RMSE of 1.94 m/s and a R^2 of 0.83 seemed to indicate a good similitude between the control run and the measurements in the validated period.
The average vertical wind profile shown in 5.1.2(a) also indicates a reasonable adjustment at almost every measured level. Even though there are discrepancies around 30 to 40m a.s.l., those differences are not observed at higher heights and the Bias is lower than 0.5m/s in every level. Remembering that the measurements at the 70m level are extrapolated, a small part of the obtained Bias might result from the extrapolation.
Monthly and hourly[2] figures are represented to find out if there are significant temporal variations in the wind speed. The first analysis might help detect seasonal variations and the second analysis is useful to observe the hourly behaviour of the wind speed. The average monthly wind speed can be seen in figure 5.1.2(b) and the hourly average wind speed is seen on figure 5.1.3(a). The good adjustment between predictions and measurements in figure 5.1.2(b) indicates no significant seasonal variations in the accuracy of the simulations. Regarding the daily pattern, even though the simulations and measurements seem to have similar shapes, the results indicate that the behaviour is not constant throughout the day. The Bias, MAE and RMSE, represented in table 5.1.2, are minimum during day hours and maximum during night hours, and the correlation is higher during day hours.
The wind roses at the mast are plotted in figure 5.1.4. Both have similar shapes and the predominant sectors seem to be properly identified.
The distribution of the wind speeds has a very good adjustment to the Weibull distribution (figure 5.1.3(b)). An error of -1.83% is obtained in the shape of the Weibull distribution and 4.2% in the scale.
Taking into account all the validations, it seems that the WRF model is able to properly simulate the particularities of the wind speed at the local of interest and generate a solid wind speed reference database to be later used to determine the wind speed deficit.

5.2 Far Wakes

In this section, the results for the Sim1 and Sim2 experiments are presented. As expected, the presence of the HR1 and HR2 have an influence in the mean wind speeds recorded in the proximity of both wind farms. The radius of influence of the far wakes generated by each wind farm appear to be long enough to affect the other downstream wind farm.

[2] Even though they are referred as monthly and hourly averages, the wind speeds illustrated in the figures are obtained from the selected period of the typical year. This means that the number of records used to obtain the wind speed average in each point is variable.

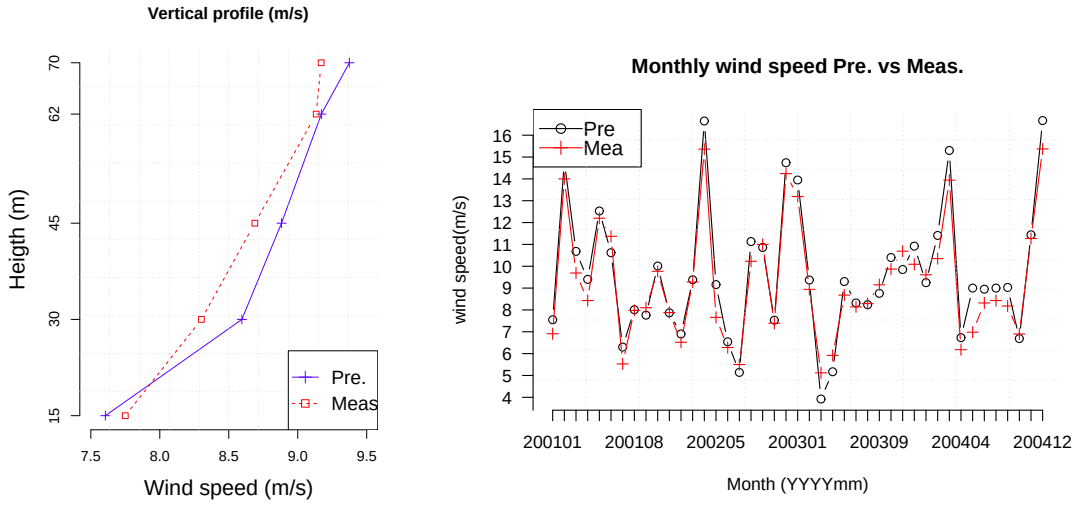

(a) Vertical profile **(b)** Monthly analysis

Figure 5.1.2: Average vertical wind profile comparison between the control run and the measurements in the M2 mast (left) and average monthly predicted and measured wind speed at 70m a.s.l. (right)

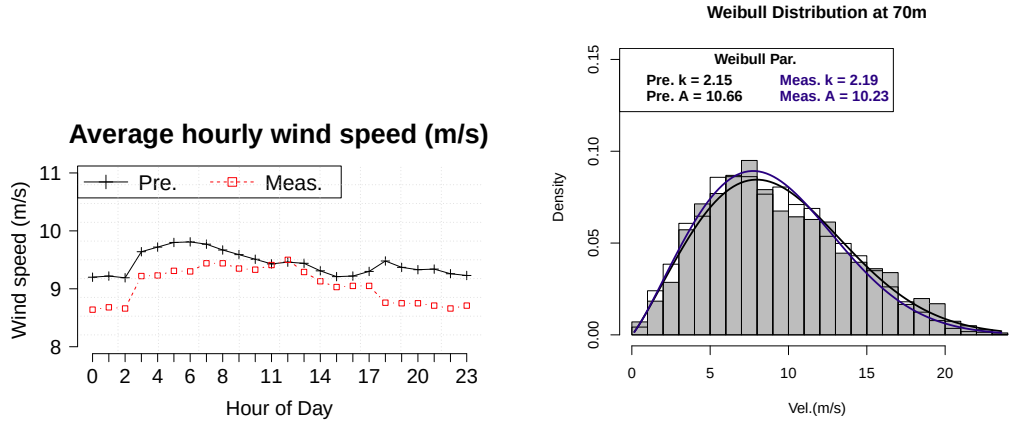

(a) Daily Pattern **(b)** Weibull

Figure 5.1.3: Predicted and measured average daily cycles (left) and weibull fit (right) at 70m a.s.l.

The mean wind speed deficit, calculated in equation 5.2.1, is used to ascertain the impact of the far wake effects in the region of interest. This value establishes a relation between the wind speed from the unperturbed state of the atmosphere (*control run*) and each of the WRF wake simulations. The wind speed deficit percentage results exclusively from the presence of the neighbour wind farm, thus providing an easy method to calculate the far wake effects.

$$MeanWSD = \left(\frac{Ws_{control} - Ws_{wakes}}{Ws_{control}} \right) * 100 \tag{5.2.1}$$

Hour	Bias	MAE	RMSE	R^2	Mean Wind Pred.	Mean Wind Meas.
0	0.57	1.69	2.37	0.76	9.2	8.64
1	0.55	1.56	2.08	0.82	9.22	8.68
2	0.53	1.59	2.16	0.81	9.19	8.66
3	0.42	1.2	1.57	0.91	9.64	9.22
4	0.49	1.25	1.55	0.91	9.72	9.23
5	0.49	1.35	1.73	0.89	9.8	9.31
6	0.52	1.4	1.93	0.86	9.81	9.3
7	0.32	1.23	1.68	0.88	9.77	9.44
8	0.23	1.25	1.69	0.88	9.67	9.44
9	0.24	1.28	1.67	0.88	9.59	9.35
10	0.19	1.36	1.69	0.87	9.51	9.33
11	0.02	1.31	1.61	0.89	9.43	9.41
12	-0.04	1.36	1.74	0.87	9.46	9.5
13	0.15	1.25	1.58	0.89	9.44	9.29
14	0.17	1.46	1.84	0.84	9.31	9.13
15	0.18	1.36	1.76	0.85	9.21	9.03
16	0.17	1.34	1.67	0.86	9.22	9.05
17	0.25	1.61	2.09	0.78	9.3	9.05
18	0.72	1.9	2.55	0.7	9.48	8.76
19	0.62	1.61	2.13	0.79	9.37	8.75
20	0.58	1.55	2.25	0.75	9.33	8.75
21	0.63	1.45	2.21	0.76	9.34	8.71
22	0.59	1.57	2.21	0.77	9.26	8.66
23	0.52	1.64	2.29	0.76	9.23	8.71

Table 5.1.2: Average hourly predicted and measured wind speed for the control run.

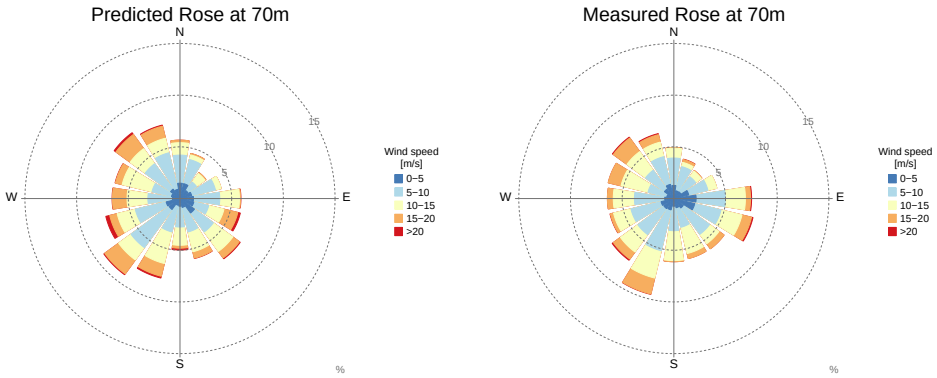

(a) Wind rose - control **(b)** Wind rose - M2

Figure 5.1.4: Wind roses for the control run (left) and the M2 mast (right) at 70m a.s.l.

where $Ws_{control}$ is the wind speed from the control run and Ws_{wakes} is the wind speed from the WRF simulations using real wind turbine positions and specifications.

5.2.1 SIM1: ONLY HR1

In this configuration, only the HR1 wind farm is considered. The wind farm parameterization is activated in the WRF innermost domain and real wind turbine characteristics and positions for the HR1 wind farm are used. The same period and domain setup are simulated.
The layout used in this simulation emulates the 2005 to 2009 period in which only the HR1 wind farm was operational. Measurements from the M6 and M7 masts, available in this period, are used to validate the simulation outputs. The validation focus only in the HR1 far wakes and tries to deduce the robustness of the mesoscale model wind farm parameterization. The global errors obtained in the validated period are presented in table 5.2.1.

Mast	Bias	MAE	RMSE	R^2	Error(%)
M6	-0.13	1.37	1.86	0.77	-1.37
M7	-0.03	1.39	1.85	0.78	-0.31

Table 5.2.1: Global errors at M6 and M7 masts in the period between 2005 and 2009.

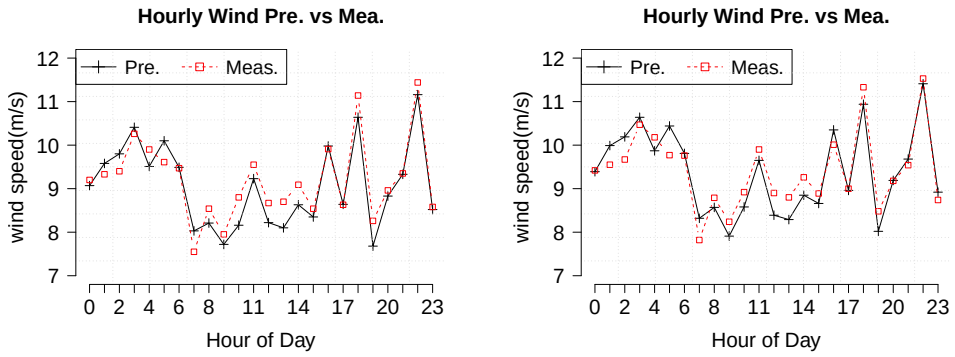

(a) M6 **(b)** M7

Figure 5.2.1: Hourly mean wind speed for the M6 and M7 masts at 70m a.s.l.

The global errors are similar in both masts. A Bias lower than -0.15 m/s and a correlation over 0.75 at both masts are recorded. The hourly predicted and measured wind speeds for both masts presented in figure 5.2.1 confirms the consistency between simulations and measurements.
The global wind speed deficits at 70 and 80m a.s.l. are show in figures 5.2.2(a) and 5.2.2(c). Both figures display an area surrounding the HR1 wind farm suffering from a decrease in the mean wind speed. The wind speed deficit in that area reaches its maximum next to the HR1 wind farm and decreases with the distance to the wind farm. Despite of the distance between the two wind farms, the far wake effects generated by the HR1 wind farm still cause a decrease of approximately 1% in the mean wind speeds recorded at the location of the HR2 wind farm.
The wind speed deficit of 1% is obtained by the hourly outputs average from the Sim1. These outputs consider the entire set of wind directions even though the far wake effects reaching the HR2 wind farm only occur in a particular sector.

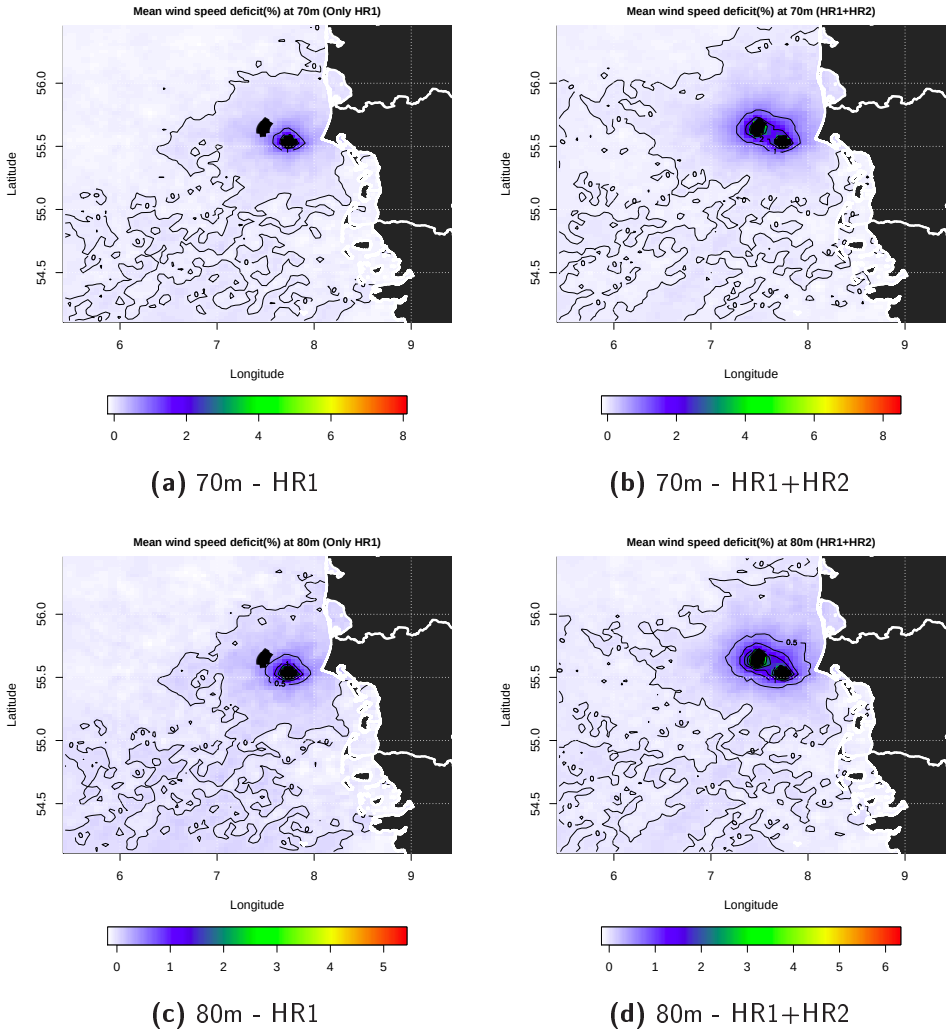

(a) 70m - HR1

(b) 70m - HR1+HR2

(c) 80m - HR1

(d) 80m - HR1+HR2

Figure 5.2.2: Mean wind speed deficit(%) for HR1 only (left) and both wind farms(right) at several heights a.s.l.

Using the available measurements from the M6 and M7 masts and selecting only the wind directions from the "WEST" sector ($255° \leq \theta \leq 285°$) it is possible to validate the wind farm parameterization and its effects on the wind speed in a point located near the wind farm (M6) and another located further downstream (M7). A subset of records is created, and the data from a cross section intersecting the entire wind farm at the masts latitudes is extracted. This way, it is possible to observe the behaviour of the wind speed as it flows through the complete length of the wind farm and the two measurement masts.

Figure 5.2.3 shows the wind speeds from the "WEST" sector in the fourth row of the HR1 wind farm and the M6 and M7 masts. The black line represents the wind speed from the reference run, the red line represents the wind speed from the wind farm parameterization run and the green points are the average measured wind speeds at the M6 and M7 masts.

The first noticeable aspect it's the equal wind speed at some adjacent wind turbines inside the wind farm. WRF 's domain resolution is lower than the distance between consecutive wind

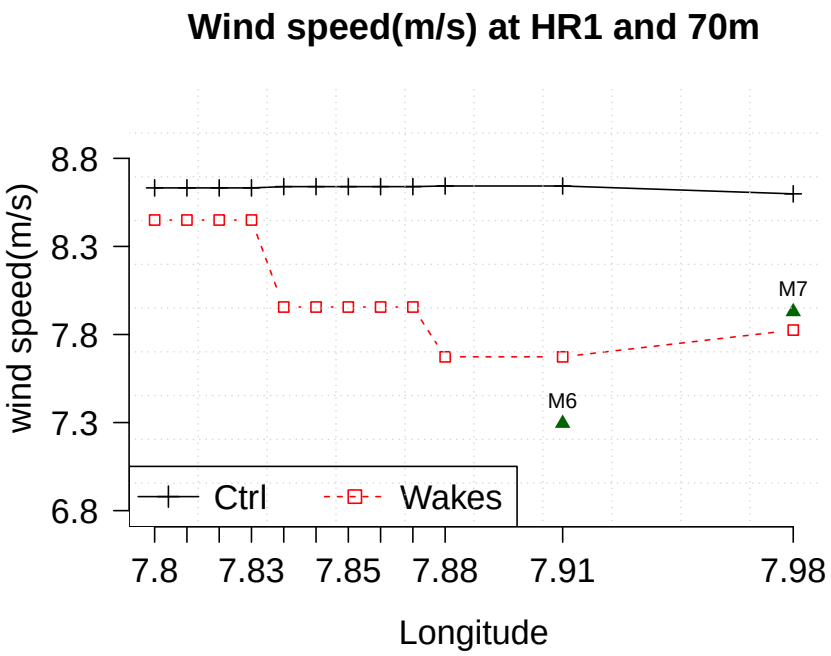

Figure 5.2.3: Wind speed in a horizontal line across the HR1 wind farm at the same latitude that the M6 and M7 masts

turbines causing that all the machines contained in the interior of the same grid cell to have the same wind speed. A consequence of this situation is the difference between the wind speed from the reference run and from Sim1, that can be observed in the first wind turbine. This turbine is located in the first column of the HR1 layout and should not suffer any wake effects since there are no turbines upstream its location. Nevertheless, the lower wind speed recorded in this turbine results from the average wind speed deficit from the other wind turbines located in the same domain cell.
For this reason, it was stated before that this methodology should be used to simulate far wake effects from the entire wind farm and not the discretization of individual wake effects from single wind turbines.

The error in the M6 mast is approximately 5-6% while in the M7 mast is about 1-2%. The distance from the M6 mast and the last column of turbines is less than 5D, so the mast could still be affected by tip and rotor vortices which are not taken into account in the WRF wind farm parameterization.
Regarding the M7 mast, its distance to the last column of turbines is big enough for the model to neglect the near wake effects and the obtained wind speed deficit is the result of the far wake effects only. At this point, the relatively low resolution of the domain stops being an issue and the wind farm parameterization is able to better adjust to the measurements.
Since the methodology was developed having similar distances in mind, it could provide a useful tool when:

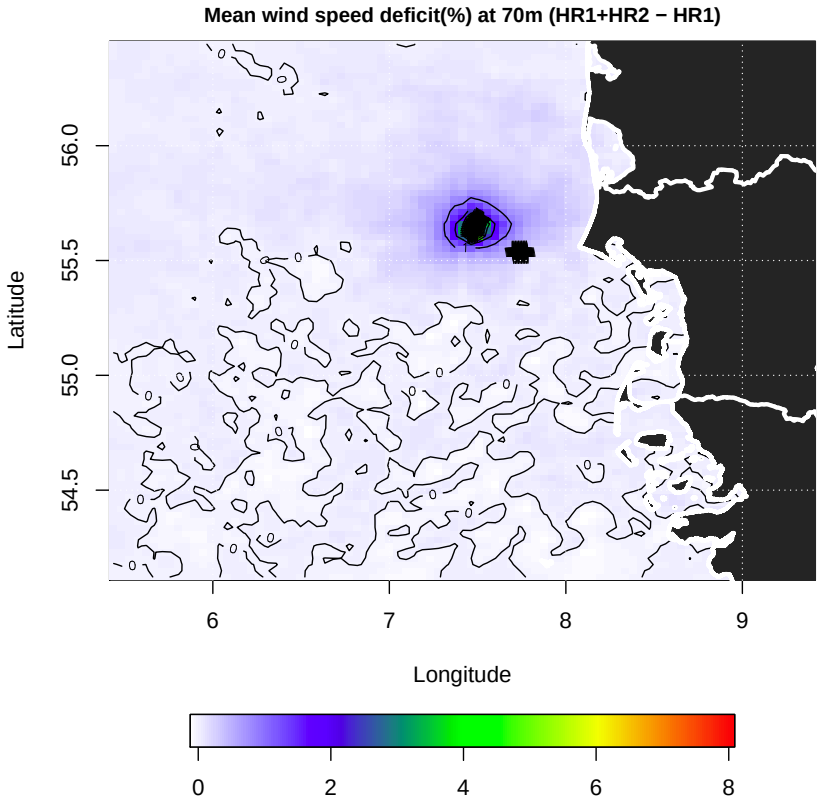

Figure 5.2.4: Wind speed deficit(%) generated by the HR2 wind farm.

- Client wants to find the optimal location for a new park in a area with pre-existent wind farms.

- Client wants to predict the wake losses at his wind farm resulting from the construction of a new wind farm in its vicinity.

5.2.2 SIM2: HR1 AND HR2

The final simulation includes both HR1 and HR2 wind farms. Real wind turbine characteristics and positions for both wind farms are used and the same period than the previous run is simulated.
Figures 5.1.1(e) and 5.1.1(f) show the mean wind speed in the entire typical year. The diminution in the wind speed around both wind farms is clearly visible, specially in the area comprehended between the two wind farms. In this region the wind speed deficit is the sum of the far wakes effects from the HR1 and HR2 wind farms.
Figures 5.2.2(b) and 5.2.2(d) illustrate the mean wind speed deficit for this configuration. The deficit resulting from the presence of both wind farms is higher than in the previous simulation and can reach average values of around 2%.
In order to quantify the wind speed deficit provoked by the inclusion of the HR2 wind farm, the wake effects from the HR1 wind farm are eliminated. The final wind speed deficit is

obtained by equation 5.2.2 and represented in figure 5.2.4.

$$WSD_{HR2} = WSD_{HR1+HR2} - WSD_{HR1} \tag{5.2.2}$$

where $WSD_{HR1+HR2}$ is the mean wind speed deficit from Sim2 and WSD_{HR1} is the mean wind speed deficit from Sim1.

The figure indicates a wind speed deficit at the HR1 wind farm around 0.5%. As stated before, this value is an average of the entire spectrum of wind directions. Accordingly to the wind rose in figure 5.1.4, only in less than 25% of occurrences a wake generated in the HR2 wind farm will affect the HR1 wind farm, thus the relatively low wind speed deficit.

Looking at some specific sectors which are known to produce far wakes on the other downstream wind farm, it is possible to see that the wind speed deficit can reach higher values. The sectors ESE, WNW and NW, with 22.5° each, are represented in figures 5.2.5(b), 5.2.5(d) and 5.2.5(c) respectively. The wind speed deficit in these cases can reach 6-8% which result in significant power losses in the downstream wind farm.

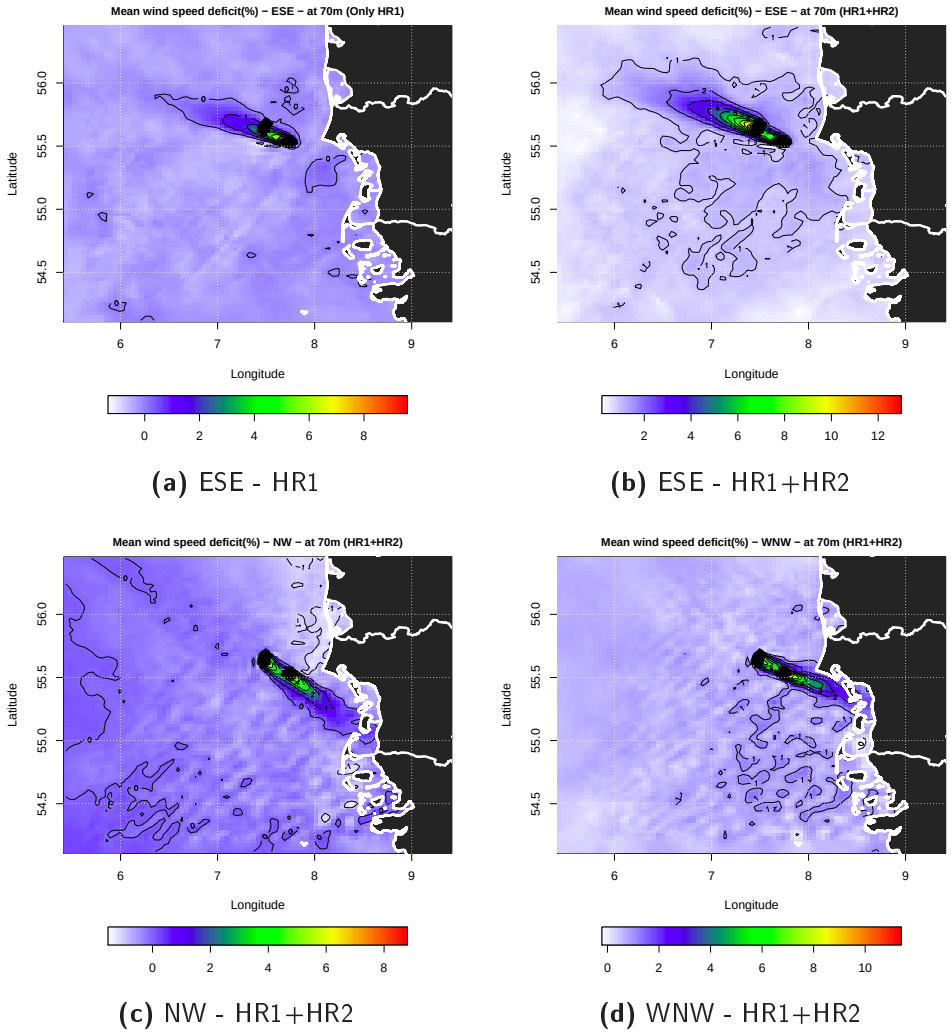

(a) ESE - HR1

(b) ESE - HR1+HR2

(c) NW - HR1+HR2

(d) WNW - HR1+HR2

Figure 5.2.5: Mean wind speed deficits(%) for several sectors and WRF configurations.

5.3 POWER PRODUCTION

The wind power generated by a wind turbine is proportional to the wind speed cubed as indicated in equation 5.3.1:

$$Power = \frac{1}{2}\rho k c_p A v^3 \tag{5.3.1}$$

where ρ is the air density, k is a constant to yield power in kilowatts, c_p is the maximum power coefficient, A is the rotor swept area and v is the wind speed.

That means that a small deficit in the wind speed might translate to a significant deficit in the power production.

Kurt Hansen's dataset includes wind power production from every wind turbine in the HR1 wind farm. Each time series includes a "quality" flag that indicates if the measurement is valid or if it suffered some kind of perturbation. Stop and start sequences of machines, power limitations from the wind farm control center and maintenance tasks, among others, have a direct influence in the measurements. Numerical simulations cannot take those constraints into account, so the original database is filtered in order to include only the valid measurements that can be compared against the mesoscale model predictions. Once the data is filtered, the 10 minutes records are averaged to hourly measurements, creating the wind power time series for every wind turbine that will be used to perform the validations.

At the same time, the hourly wind speed time series from the mesoscale simulations in each machine position at the HR1 wind farm are converted to wind power. The theoretical power curves from each wind turbine (figure 4.2.1) are used to transform the wind speed time series into wind power.

Figure 5.3.1 shows the mean wind power for every HR1 machines obtained from Sim1. Figure 5.3.2 illustrates the measured mean wind power for the same period.

Comparing both figures, clearly shows that the mesoscale model overestimates the wind power at the HR1 wind farm. There are three possible reasons for this overestimation, the first being that the wind farm parameterization might be underestimating the wake effects from the wind turbines, the second might be the low resolution of the domain and the third could be that the theoretical power curve used to convert the wind speed to power tends to overestimate the production. Generally the theoretical power curves provided by the wind turbine manufacturers always slightly overestimate the turbine wind power production. Wear and tear of the blades and mechanical components, erosion provoked by the weather conditions and the salt from the ocean water contribute to a lower power productions than the theoretical power curve indicates. Taking that into consideration, it is still possible to observe that the wind turbines located on the Southern and Western frontiers seem to register the highest productions. Being located in the outer border of the wind farm, those machines do not suffer any wake effects when having Southerly winds (Southern border) of Westerly winds (Western border).

At this point, it is possible to compare the measured and the simulated wind power times series and calculate the errors at every machine position. Table 5.3.1 shows the Bias, MAE, RMSE, R^2

Turb	Bias	MAE	RMSE	R^2	Error	Turb	Bias	MAE	RMSE	R^2	Error
T01	22.71	248.21	383.27	0.73	2.04	T51	65.76	252.97	378.06	0.74	6.29
T02	44.38	246.68	374.94	0.74	4.04	T52	93.11	255.39	382.46	0.74	9.09
T03	43.61	244.44	374.2	0.75	3.96	T53	98.63	262.68	384.15	0.74	9.81
T04	35.81	242.96	368.76	0.75	3.33	T54	82.81	258.3	381.06	0.74	8.22
T05	40.99	244.03	373.04	0.75	3.76	T55	78.87	251.41	375.71	0.75	7.9
T06	34.95	247.63	382.24	0.74	3.24	T56	76.78	247.34	372.27	0.75	7.56
T07	33.92	245.18	371.99	0.74	3.13	T57	49.1	240.72	369.41	0.75	4.7
T08	55.01	246.33	380.54	0.74	4.82	T58	120.53	278.78	413.12	0.71	11.7
T11	66.54	254.29	377.36	0.74	6.23	T61	67.91	252.36	376.15	0.74	6.65
T12	85.22	261.96	387.93	0.73	8.08	T62	82.39	256.3	384.52	0.73	8.06
T13	83.5	260.2	387.72	0.73	7.86	T63	97.74	269.19	391.19	0.73	9.63
T14	84	256.38	386.96	0.74	7.82	T64	95.72	262.67	387.01	0.73	9.31
T15	80.45	251.78	380.07	0.74	7.56	T65	88.15	251.79	373.8	0.75	8.5
T16	75.14	249.45	378.74	0.75	7.03	T66	65.42	248.6	374.78	0.74	6.36
T17	62.75	249.61	379.4	0.74	5.88	T67	65.42	248.6	374.78	0.74	6.36
T18	71.44	247.36	373.56	0.75	6.38	T68	94.21	264.83	400.71	0.72	8.61
T21	67.84	253.55	381.07	0.74	6.35	T71	68.78	261.23	387.64	0.73	6.47
T22	95.93	262.73	394.59	0.73	9.08	T72	84.61	268.68	397.62	0.72	8.13
T23	106.75	266.56	396.21	0.73	10.22	T73	66.95	259.14	385.69	0.73	6.51
T24	101.53	261.3	390.67	0.73	9.67	T74	80.31	260.63	383.46	0.73	7.7
T25	87.83	254.44	385.13	0.74	8.37	T75	97.96	273.51	401.25	0.71	9.75
T26	94.81	260.95	392.52	0.73	9.23	T76	53.59	248.1	372.6	0.74	5.16
T27	63.9	254.39	388.09	0.73	5.94	T77	49.4	244.4	370.95	0.75	4.72
T28	95.24	257.3	391.14	0.73	8.52	T78	104.4	261.41	398.26	0.72	9.19
T31	91.7	267.18	398.92	0.72	8.78	T81	61.06	269.97	402.12	0.7	5.77
T32	124.22	264.59	387.05	0.75	12.59	T82	73.63	266.37	397.16	0.72	7.01
T33	140.59	280.56	420.27	0.71	13.48	T83	65.91	264.68	392.9	0.72	6.39
T34	126.96	271.11	402.72	0.73	12.28	T84	67.47	261.49	387.62	0.73	6.58
T35	79.41	246.23	368.49	0.76	7.55	T85	64.05	256.6	383.88	0.73	6.27
T36	77.11	242.74	364.09	0.76	7.43	T86	52.65	261.54	391.82	0.72	5.06
T37	37.1	241.65	364.73	0.75	3.57	T87	63.08	245.52	372.24	0.75	5.96
T38	90.37	265.29	397.02	0.72	8.33	T88	90.21	261.48	395.96	0.72	8.31
T41	69.24	258.09	385.89	0.73	6.72	T91	38.23	259.81	390.28	0.72	3.59
T42	90.64	259.32	387.61	0.73	8.97	T92	85.37	263.85	393.64	0.72	7.94
T43	76.81	258.2	382.35	0.73	7.62	T93	80.59	257.4	381.03	0.74	7.65
T44	93.92	255.05	374.76	0.75	9.15	T94	75.23	256.14	382.94	0.73	7.06
T45	69.06	252.18	373.16	0.75	6.87	T95	79.47	255.01	379.74	0.74	7.54
T46	66.93	245.45	370.17	0.75	6.52	T96	57.1	240.32	363.24	0.76	5.43
T47	63.07	244.92	372.5	0.75	5.95	T97	57.82	239.84	365.88	0.75	5.3
T48	83.56	259.53	395.93	0.73	7.69	T98	33.33	246.56	370.09	0.74	2.98

Table 5.3.1: Global Errors at each wind turbine in HR1 taking into account only the HR1 wind farm.

and the percentage error for each wind turbine in Sim1. Even though the domain resolution is not the ideal to perform this type of analysis, the results seem promising. A mean error of 7.1%, combined with a correlation over 0.7 in all wind turbines indicate that the wind farm parameterization could be useful to obtain a rough estimate on wind energy production, even at this resolution.

Figure 5.3.4 represents the error from Sim1 in every wind turbine from HR1 . The error at turbines T32, T33 and T34 reaches its maximum. Since several wind turbines are located inside the same grid cell, the wind speed differences that occur between consecutive

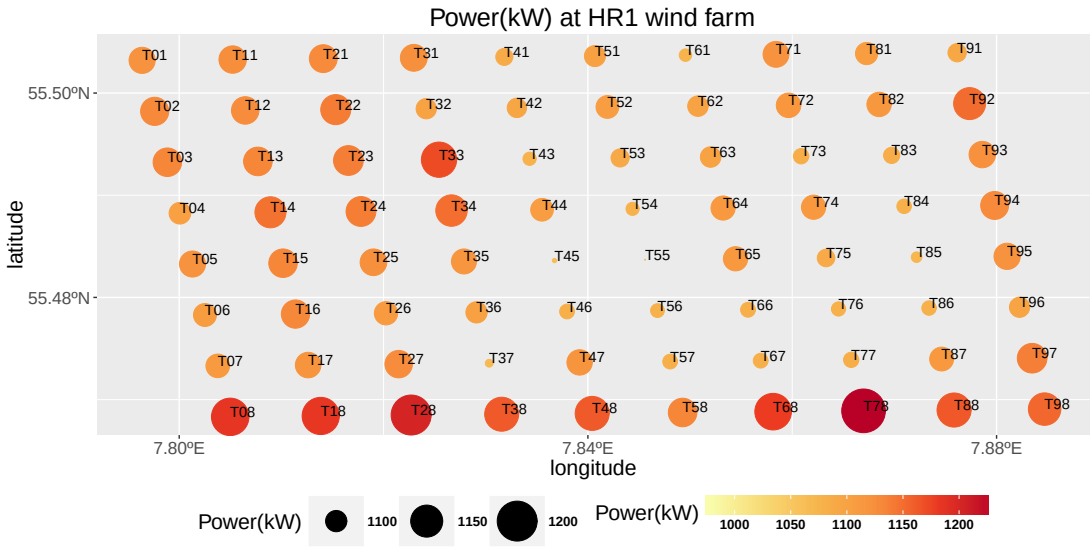

Figure 5.3.1: Mean wind power(kW) in all wind turbines at the HR1 wind farm from Sim1.

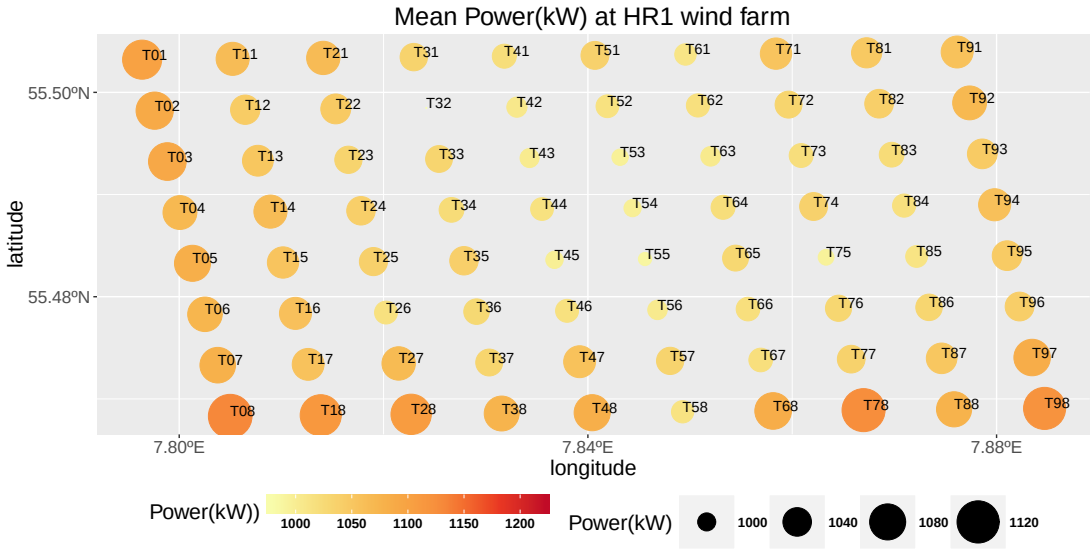

Figure 5.3.2: Mean wind power(kW) in all wind turbines at the HR1 wind farm obtained from the measurements.

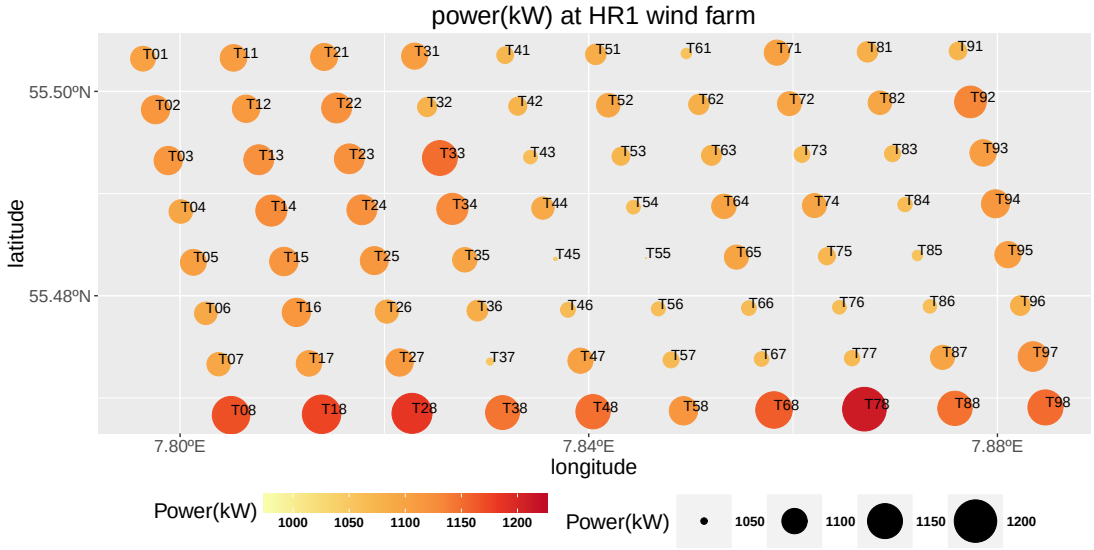

Figure 5.3.3: Power(kW) in all wind turbines at the HR1 wind farm from Sim2.

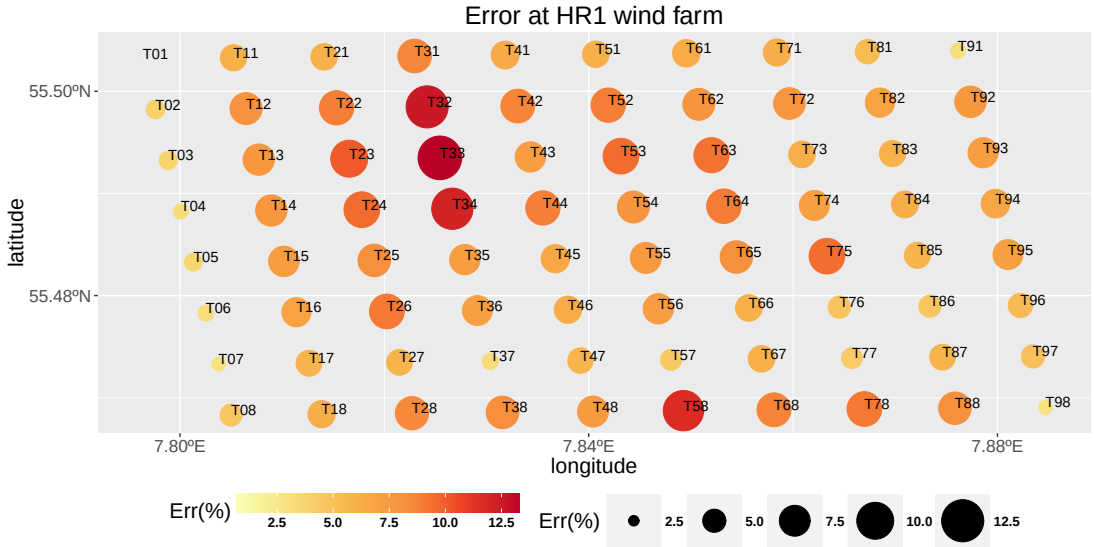

Figure 5.3.4: Error(%) in all wind turbines at the HR1 wind farm from Sim1.

machines is not properly simulated, resulting in higher errors in some of the turbines.
Looking now at the the mean wind power from Sim2 represented in figure 5.3.3 it is noticeable that there is a slightly decrease in the mean predicted wind power due to the far wake effects from the HR2 wind farm.
Sim1 predicted an average wind power production of 1127.49kW, while the Sim2 predicted 1105.37kW, which represents a deficit of 1.96%.Even though the deficit appears to be relatively low, due to the sheer size of offshore wind farms, a power production deficit of this magnitude can result in important economic costs.
Calculating the theoretical wind power production by selecting only the wind speed from the "NW" sector, where the influence of the HR2 wind farm in the HR1 appears to be maximum, will allow to observe the maximum theoretical wind power deficit at the HR1 wind farm. The wind speeds from the "NW" sector are selected and transformed into wind power production following each turbine's power curve. The average wind power production of every wind turbine is represented in table 5.3.2. An average wind power production of 1120.81kW is obtained from Sim1 and an average wind power production of 1071.78kW is obtained in Sim2, resulting in a 4.37% mean wind power deficit at the HR1 wind farm when the "NW" sector is selected. As expected, it is higher than the total deficit calculated before. In cases where there is more than one neighbouring wind farm, the losses due to far wake effects can reach significant values and become a major factor when deciding the position and layout of new wind farms.
These results reaffirm the importance of this type of study in areas with high concentrations of wind farms or in locations near large upstream wind farms. In this case, despite having only two wind farms included in the study, the obtained wind speed and wind power deficits are already significant which means that in other areas, the presence of neighbour wind farms can cause significant monetary losses at nearby downstream wind farms.

Turbine	Wind Power-Sim1 (kW)	Wind Power-Sim2 (kW)	Turbine	Wind Power-Sim1 (kW)	Wind Power-Sim2 (kW)
T01	1160.29	1119.57	T51	1137.11	1111.19
T02	1155.18	1088.19	T52	1137.11	1111.19
T03	1155.18	1088.19	T53	1087.27	1034.20
T04	1155.18	1088.19	T54	1087.27	1034.20
T05	1155.18	1088.19	T55	1087.27	1034.20
T06	1155.18	1088.19	T56	1087.27	1034.20
T07	1155.18	1105.82	T57	1087.27	1034.20
T08	1189.90	1129.86	T58	1114.05	1073.60
T11	1160.30	1119.57	T61	1137.11	1111.19
T12	1155.18	1088.19	T62	1137.11	1111.19
T13	1155.18	1088.19	T63	1087.27	1034.20
T14	1155.18	1088.19	T64	1087.27	1034.20
T15	1155.18	1088.19	T65	1087.27	1034.20
T16	1155.18	1088.19	T66	1087.27	1034.20
T17	1155.18	1088.19	T67	1087.27	1034.20
T18	1189.86	1129.86	T68	1114.05	1073.60
T21	1160.30	1119.57	T71	1137.11	1111.19
T22	1155.18	1088.19	T72	1137.11	1111.19
T23	1155.18	1088.19	T73	1087.27	1034.20
T24	1155.18	1088.19	T74	1087.27	1034.20
T25	1155.18	1088.19	T75	1087.27	1034.20
T26	1155.18	1088.19	T76	1087.27	1034.20
T27	1155.18	1088.19	T77	1087.27	1034.20
T28	1189.86	1129.86	T78	1114.05	1073.60
T31	1160.30	1119.57	T81	1137.11	1111.19
T32	1160.30	1119.57	T82	1137.11	1111.19
T33	1155.18	1088.19	T83	1087.27	1034.20
T34	1155.18	1088.19	T84	1087.27	1034.20
T35	1087.27	1034.20	T85	1087.27	1034.20
T36	1087.27	1034.20	T86	1087.27	1034.20
T37	1087.27	1034.20	T87	1073.93	1045.37
T38	1114.05	1073.60	T88	1075.72	1030.86
T41	1137.11	1111.19	T91	1137.11	1111.19
T42	1137.11	1111.19	T92	1160.49	1142.65
T43	1087.27	1034.20	T93	1073.93	1045.37
T44	1087.27	1034.20	T94	1073.93	1045.37
T45	1087.27	1034.20	T95	1073.93	1045.37
T46	1087.27	1034.20	T96	1073.93	11045.37
T47	1087.27	1034.20	T97	1073.93	1045.37
T48	1114.05	1073.60	T98	1075.72	1030.87

Table 5.3.2: Average theoretical wind power production in each wind turbine from HR1 wind farm for the Sim1 and Sim2, selecting only the directions from the “NW” sector.

CHAPTER 6

CONCLUSIONS

The objective of this work was to obtain a "low-cost" methodology that could make use of the latest mesoscale model developments regarding the simulation of wake effects in offshore wind farms. This methodology would allow a possible client to obtain a faster and computationally less costly than traditional microscale wake models, analysis of a given area comprised within the radius of influence of neighbouring wind farms. Depending on the number and size of neighbour wind farms, such an analysis could save money and time and might prove a determining factor in decision making.

Three mesoscale simulations using the WRF model were performed in the Horns Rev region. A simulation without the presence of wind farms provided the reference wind climate of the region, a second simulation was performed using the real HR1 wind turbine characteristics and positioning and finally, a third simulation, using real wind turbine characteristics and positioning for the HR1 and HR2 was conducted. Measurements from three masts and from individual wind turbines in the HR1 wind farm created an invaluable measurements database used to validate the methodology.

The wind climate obtained from the control run and validated in the M2 mast indicates that the region has a high mean wind speed of over 9m/s at 70m a.s.l.. The mean wind speed validation calculated a global R^2 of 0.83 and a Bias of 0.38m/s that results in an error of 4.2%. The wind roses, daily pattern and monthly error analysis all seem to indicate that the mesoscale model was able to properly capture the wind characteristics of the region.

Considering the relatively low errors, the wind climate can be used with a certain degree of confidence as the reference for the unperturbed wind speed when calculating the wind speed deficits.

The results from Sim1 are used to validate the wind farm parameterization from the WRF model in the 2005-2009 period. Masts M6 and M7 are located downstream from the HR1 wind farm and have available wind speed and direction measurements that can be used to determine the far wake effects produced by the presence of the HR1 wind farm.

The global errors for the two masts in the 2005-2009 period indicated a Bias of -0.13m/s in the M6 mast and -0.03m/s in the M7 mast. A coefficient of determination of 0.77 and 0.78 for the M6 and M7 masts confirm the good adjustment between predictions and measurements. The

results in both masts are similar since there has been no selection of particular wind directions when performing the validation. It means that only in a small percentage of situations (westerly winds) where the far wake effects felt at the M6 and M7 masts. In order to properly observe the far wake effects at both masts, only the wind speeds from the "West" sector were represented in a cross-section, at the masts latitude, that passed through the HR1 wind farm and both masts. The resulting figure should make possible to see the wind speed decrease between consecutive wind turbines in the same row and the recovery of the wind speed after the wind farm. As stated in previous sections, the cross-section confirmed that this domain resolution does not allow to discern variations between consecutive wind turbines. Theoretically, no wind speed deficit should be recorded in the first wind turbine, but the equal wind speeds in the first four wind turbines of the cross-section show otherwise. Since all four machines are contained in the same grid cell, the wind speed deficit caused by the wake effects from the individual turbines is averaged and attributed to all machines inside that cell.
Downstream from the wind farm, the wind speed starts to recover, and the wind speed errors at the M6 and M7 masts are around 5-6% and 1-2% respectively. The distance between the M7 mast and the wind farm is big enough for the domain resolution to stop being a major factor in the wake simulation, hence the lower error than at the M6 mast.
The Sim2 shows a wide area surrounding both HR1 and HR2 that is affected by far wake effects from both wind farms. HR2 wind farm generates a mean wind speed deficit around 0.5% on the HR1 wind farm. The magnitude of the wind speed deficit is not significant when looking at the mean wind resource assessment, but when determined sectors are studied, the wind speed deficit can reach 8%.
The high wind speed deficits in certain wind directions might have a significant impact in the total instantly production of the wind farm in situations of prolonged winds from a given sector. The owners of every wind farm need to provide the electrical market with daily forecasts for the wind power production. Any deviations between the forecasts and the real production of the wind farm leads to fines that can be very costly in some cases. A useful application for this methodology might be to create a reference table constituted by the pre-calculated wind speed deficits for several bins of wind speeds and directions that would be applied to perform statistical corrections of the operational power production forecasts. That way, the estimation for the wind power when the wind is blowing from these critical sectors would include the expected wake effects from the other upstream wind farms.
Even if this methodology in not the most adequate to obtain the power production estimation of a wind farm, since we are working with typical mesoscale resolutions[1] that are not appropriate to this type of use, a validation of the simulations against real measurements at each turbine was made. The goal was to ascertain if it was possible to obtain a very rough estimation of the impact of the wake effects from the HR2 in the HR1 wind farm power production.
First, the Sim1 results were compared with the available measurements in the HR1 wind farm to calculate the magnitude of the error between the predicted and measured wind power.

[1] usual between 1 and 10km

Since the mesoscale model cannot capture all the particularities of the wind turbine operation, only the measurements that were classified as "valid" were used. This way, start and stop sequences of machines as well as bad and invalid measurements were eliminated from the final database. The simulated wind speed was converted to power using each machine theoretical power curves. A mean error of 7.1% and a R^2 over 0.7 seem to indicate that the wind power estimation might be useful in a preliminary stage of the wind farm development.
Finally, the Sim1 and Sim2 power estimations were compared and a wind power deficit of 1.96% on the HR1 wind farm, provoked by the HR2 wind farm, was obtained. The deficit increased to 4.37% when selecting only the wind directions from the "NW" sector.
The relatively low wind speed and power deficit obtained in this study results from having a low concentration of wind farms in the studied region. Other studies conducted in areas with a much higher concentration of wind farms indicated that the wind speed deficits can reach much higher values. One of the work packages in the EERA-DTOC project conducted the simulation of two test cases corresponding to a base and near future scenario. The first test case was conducted taking into account the Race Bank[2] wind farm that is already in a pre-construction phase and second test case took into account the Dogger Bank location in which four major wind farms have been granted the consent to build and that would represent a near future scenario. The WRF simulations by CENER, carried out in that test case taking into account only the neighbour wind farms and later adding the target wind farm, showed wind speed deficits that could reach 4% in the first case and 8% in the second (Schepers et al., 2015). Those results have shown that in a near future, as the number of wind farms keeps increasing, this type of study might prove invaluable in some areas with higher concentration of wind farms.
As a final conclusion, it seems that the methodology can provide useful information in a pre-construction phase of a project as well to study the impact of future wind farm constructions in the vicinity of an already existing wind farm. Since the model domain resolution is relatively low in order to provide fast results, decisions regarding the layout of a offshore wind farm should not be made based solely on the results from this approach.

[2] http://www.4coffshore.com/windfarms/windfarms.aspx?windfarmId=UK18

REFERENCES

Cabezón, D., J. Sanz, I. Martí, and A. Crespo (2009). "CFD modelling of the interaction between the Surface Boundary Layer and rotor wake." In: Stockholm, Sweden: European Wind Energy Conference (cit. on p. 25).

Chavez-Arroyo, R. (2014). "Novel approaches to the efficient modelling of the long-term mesoscale wind resource." PhD thesis. University of Monterrey (cit. on pp. 30, 31, 33, 34).

Chavez-Arroyo, R., P. Correia, J. Amezcua, S. Lozano, O. Probst, and J. Sanz (2015). "A novel approach to statistical dynamical downscaling for long-term wind resource predictions." In: *Applied Thermal Engineering* In Press (cit. on p. 30).

Chen, F. and J. Dudhia (2001). "Coupling and advanced land surface-hydrology model with the Penn State-NCAR MM5 modeling system. Part I: model implementation and sensitivity." In: *Monthly Weather Review* 129.4, 569–585 (cit. on p. 36).

Christiansen, M. B. and C. B. Hasager (2005). "Wake effects of large offshore wind farms identified from satellite SAR". In: *Remote Sens. Environm.* 98, pp. 251–268. DOI: 10.1016/j.rse.2005.07.009 (cit. on p. 27).

Dee, D. P. e. a. (2011). "The ERA-Interim reanalysis: configuration and performance of the data assimilation system." In: *Quarterly Journal of the Royal Meteorological Society*. DOI: 10.1002/qj.828 (cit. on p. 36).

Dudhia, J. (1989). "Numerical study of convection observed during the winter monsoon experiment using a mesoscale two-dimensional model." In: *Journal of the atmospheric sciences* 46, pp. 3077–3107 (cit. on p. 36).

Fitch, A. C., J. Olson, J. Lundquist, J. Dudhia, A. Gupta, J. Michalakes, and I. Barstad (2012). "Local and Mesoscale Impacts Parameterized in of a Wind Farms as Mesoscale NWP Model." In: *Monthly Weather Review*. DOI: http://dx.doi.org/10.1175/MWR-D-11-00352.1 (cit. on pp. 19, 25, 28).

Fitch, A. C. (2015). "Notes on using the mesoscale wind farm parameterization of Fitch et al. (2012) in WRF". In: *Wind Energy*. we.1945. ISSN: 1099-1824. DOI: 10.1002/we.1945. URL: http://dx.doi.org/10.1002/we.1945 (cit. on p. 25).

Frandsen S., e. a. (2006). "Analytical modelling of wind speed deficit in large offshore wind farms." In: *Wind Energy* 9, pp. 39–53 (cit. on p. 25).

Hansen K.H., e. a. (2011). *Guideline to wind farm wake analysis*. Final Report, Chapter 8, ECN-E–11-013. UPWIND (cit. on p. 42).

Hansen, K. H., R. J. Barthelmie, L. E. Jensen, and A. Sommer (2010). "The impact of turbulence intensity and atmospheric stability on power deficits due to wind turbine wakes at Horns Rev wind farm." In: *Wind Energy* 15, pp. 183–196 (cit. on p. 42).

Hasager, C. B., L. Rasmussen, A. Peña, L. E. Jensen, and P. E. Réthoré (2013). "Wind Farm Wake: The Horns Rev Photo Case." In: *Energies 2013* 6, pp. 696–716. DOI: 10.3390/en6020696 (cit. on p. 23).

Hasager, C. B., P. Vincent, R. Husson, A. Mouche, M. Badger, A. Peña, P. Volker, J. Badger, A. D. Bella, A. Palomares, E. Cantero, and P. Correia (2015). "Comparing satellite SAR and wind farm wake models." In: *Journal of Physics: Conference Series, Visby Wake Conference 2015* 625 (cit. on pp. 20, 27, 28).

Ho, A., A. Mbistrova, and G. Corbetta (2016). *The European offshore wind industry - key trends and statistics 2015*. Tech. rep. European Wind Energy Association (cit. on pp. 17–19).

Hong, S. Y., J. Dudhia, and S. H. Chen (2004). "A revised approach to ice microphysical processes for the bulk parameterization of clouds and precipitation." In: *Monthly Weather Review* 132, pp. 103–120 (cit. on p. 36).

Ito, J., H. Niino, and M. N. C.-H. Moeng (2015). "An Extension of the Mellor–Yamada Model to the Terra Incognita Zone for Dry Convective Mixed Layers in the Free Convection Regime". In: *Boundary-Layer Meteorology* 157.1, pp. 23–43. ISSN: 1573-1472. DOI: 10.1007/s10546-015-0045-5. URL: http://dx.doi.org/10.1007/s10546-015-0045-5 (cit. on p. 25).

Jensen, N. (1983). *A note on wind generator interaction*. Technical Report Risoe-M-2411(EN). Roskilde, Denmark: Risø National Laboratory (cit. on p. 24).

Jha, P. K., E. P. N. Duque, J. L. Bashioum, and S. Schmitz (2015). "Unraveling the Mysteries of Turbulence Transport in a Wind Farm". In: *Energies* 8.7, p. 6468. ISSN: 1996-1073. DOI: 10.3390/en8076468. URL: http://www.mdpi.com/1996-1073/8/7/6468 (cit. on p. 24).

Jimenez, A., A. Crespo, E. Migoya, and J. Garcia (2008). "Large-eddy simulation of spectral coherence in a wind turbine wake." In: *Environ. Res. Lett.* 3. DOI: 10.1088/1748-9326/3/1/015004 (cit. on p. 22).

Kain, J. S. and J. M. Fritsch (1990). "A one-dimensional entraining/detraining plume model and its application in convective parameterization." In: *Journal of the Atmospheric Sciences* 47.2, 2784–2802 (cit. on p. 36).

Kallos, G., P. Katsafados, and A. Papadopoulos (2005). *The Weather Forecasting System SKIRON - Description of the model*. Tech. rep. (cit. on p. 31).

Kohonen, T. (1995). *Self-organizing maps*. Springer-Verlag. ISBN: 9783540679219. DOI: 10.1007/978-3-642-56927-2 (cit. on p. 30).

Larsen, G. (1983). *A Simple Wake Calculation Procedure*. Technical Report. Roskilde, Denmark (cit. on p. 25).

Mlawer, E. J., S. J. Taubman, P. D. Brown, M. J. Iacono, and S. Clough (1997). "Radiative transfer for inhomogeneous atmospheres: RRTM, a validated correlated-k model for the longwave". In: *Journal of Geophysical Research* 102, pp. 16663–16682 (cit. on p. 36).

Nakanishi, M. and H. Niino (2004). “An improved Mellor-Yamada level- 3 model with condensation physics: its design and verification.” In: *Bound.-Lay. Meteorol* 112, pp. 1–31 (cit. on p. 36).

Rife, D. L., E. Vanvyve, J. O. Pinto, A. J. Monaghan, C. A. Davis, and G. S. Poulos (2013). “Selecting Representative Days for More Efficient Dynamical Climate Downscaling: Application to Wind Energy”. In: *Journal of Applied Meteorology and Climatology* 52.1, pp. 47–63. DOI: 10.1175/JAMC-D-12-016.1. URL: http://dx.doi.org/10.1175/JAMC-D-12-016.1 (cit. on p. 31).

Schepers, G., A. Pena, A. Ely, A. Palomares, A. Attiya, G. Sieros, G. Giebel, H. Svendsen, I. Bastigkeit, I. Karagali, I. Moya, O. A. Lara, P. Ledesma, P. Correia, V. Gomez, and W. He (2015). *EERA DTOC calculation of scenarios*. Tech. rep. (cit. on p. 62).

Skamarock, W. C., J. B. Klemp, J. Dudhia, D. O. Gill, D. M. Barker, M. G. Duda, X. Y. Huang, W. Wang, and J. G. Powers (2008). *A description of the advanced research WRF version 3*. Technical note TN-475+STR. NCAR, 113pp (cit. on p. 36).

Wang, Y., L. Leung, J. L. McGregor, D. K. Lee, W. C. Wang, Y. Ding, and F. Kimura (2004). “Regional Climate Modeling: Progress, Challenges, and Prospects.” In: *Journal of Meteorological Society Japan* 82, 1599–1628. DOI: 10.1175/JAMC-D-12-016.1. URL: http://dx.doi.org/10.1175/JAMC-D-12-016.1 (cit. on p. 32).

APPENDIX A

WIND TURBINE COORDINATES

Latitude	Longitude	Machine	Latitude	Longitude	Machine
55.50320	7.79637	V80-2.0MW (Vestas)	55.49821	7.7976	V80-2.0MW (Vestas)
55.49323	7.79884	V80-2.0MW (Vestas)	55.48824	7.80007	V80-2.0MW (Vestas)
55.48327	7.8013	V80-2.0MW (Vestas)	55.47828	7.80252	V80-2.0MW (Vestas)
55.47330	7.80377	V80-2.0MW (Vestas)	55.46831	7.80499	V80-2.0MW (Vestas)
55.50328	7.80523	V80-2.0MW (Vestas)	55.49830	7.80646	V80-2.0MW (Vestas)
55.49331	7.8077	V80-2.0MW (Vestas)	55.48833	7.80893	V80-2.0MW (Vestas)
55.48335	7.81016	V80-2.0MW (Vestas)	55.47837	7.81138	V80-2.0MW (Vestas)
55.47338	7.81262	V80-2.0MW (Vestas)	55.46840	7.81385	V80-2.0MW (Vestas)
55.50337	7.8141	V80-2.0MW (Vestas)	55.49838	7.81532	V80-2.0MW (Vestas)
55.49340	7.81656	V80-2.0MW (Vestas)	55.48841	7.81779	V80-2.0MW (Vestas)
55.48344	7.81901	V80-2.0MW (Vestas)	55.47845	7.82024	V80-2.0MW (Vestas)
55.47347	7.82148	V80-2.0MW (Vestas)	55.46849	7.8227	V80-2.0MW (Vestas)
55.50345	7.82296	V80-2.0MW (Vestas)	55.49847	7.82418	V80-2.0MW (Vestas)
55.49348	7.82543	V80-2.0MW (Vestas)	55.48850	7.82665	V80-2.0MW (Vestas)
55.48352	7.82787	V80-2.0MW (Vestas)	55.47854	7.8291	V80-2.0MW (Vestas)
55.47356	7.83034	V80-2.0MW (Vestas)	55.46857	7.83156	V80-2.0MW (Vestas)
55.50354	7.83182	V80-2.0MW (Vestas)	55.49855	7.83305	V80-2.0MW (Vestas)
55.49357	7.83429	V80-2.0MW (Vestas)	55.48858	7.83551	V80-2.0MW (Vestas)
55.48361	7.83673	V80-2.0MW (Vestas)	55.47862	7.83796	V80-2.0MW (Vestas)
55.47364	7.83919	V80-2.0MW (Vestas)	55.46865	7.84042	V80-2.0MW (Vestas)
55.50362	7.84069	V80-2.0MW (Vestas)	55.49864	7.84191	V80-2.0MW (Vestas)
55.49365	7.84315	V80-2.0MW (Vestas)	55.48867	7.84437	V80-2.0MW (Vestas)
55.48369	7.84559	V80-2.0MW (Vestas)	55.47871	7.84681	V80-2.0MW (Vestas)
55.47372	7.84805	V80-2.0MW (Vestas)	55.46874	7.84927	V80-2.0MW (Vestas)
55.50371	7.84955	V80-2.0MW (Vestas)	55.49872	7.85077	V80-2.0MW (Vestas)
55.49374	7.85201	V80-2.0MW (Vestas)	55.48875	7.85323	V80-2.0MW (Vestas)
55.48378	7.85445	V80-2.0MW (Vestas)	55.47879	7.85567	V80-2.0MW (Vestas)
55.47381	7.85691	V80-2.0MW (Vestas)	55.46882	7.85813	V80-2.0MW (Vestas)
55.50379	7.85841	V80-2.0MW (Vestas)	55.49880	7.85964	V80-2.0MW (Vestas)
55.49382	7.86087	V80-2.0MW (Vestas)	55.48883	7.86209	V80-2.0MW (Vestas)
55.48386	7.86331	V80-2.0MW (Vestas)	55.47887	7.86453	V80-2.0MW (Vestas)
55.47389	7.86577	V80-2.0MW (Vestas)	55.46890	7.86698	V80-2.0MW (Vestas)
55.50387	7.86728	V80-2.0MW (Vestas)	55.49889	7.8685	V80-2.0MW (Vestas)
55.49390	7.86973	V80-2.0MW (Vestas)	55.48892	7.87095	V80-2.0MW (Vestas)
55.48394	7.87217	V80-2.0MW (Vestas)	55.47896	7.87339	V80-2.0MW (Vestas)
55.47397	7.87462	V80-2.0MW (Vestas)	55.46898	7.87584	V80-2.0MW (Vestas)
55.50395	7.87614	V80-2.0MW (Vestas)	55.49897	7.87736	V80-2.0MW (Vestas)
55.49398	7.8786	V80-2.0MW (Vestas)	55.48900	7.87981	V80-2.0MW (Vestas)
55.48402	7.88103	V80-2.0MW (Vestas)	55.47904	7.88225	V80-2.0MW (Vestas)
55.47405	7.88348	V80-2.0MW (Vestas)	55.46907	7.8847	V80-2.0MW (Vestas)

Table A.0.1: Turbine positions and type of turbine in the HornsRev 1 offshore wind farm.

Latitude	Longitude	Machine	Latitude	Longitude	Machine
55.5564930204	7.5467925748	SWT-2.3-93	55.5570259352	7.5553821081	SWT-2.3-93
55.5575492663	7.5639722117	SWT-2.3-93	55.5580809793	7.5725622281	SWT-2.3-93
55.5586031087	7.5811528103	SWT-2.3-93	55.5591336198	7.5897433086	SWT-2.3-93
55.5596545472	7.5983343681	SWT-2.3-93	55.5646041661	7.5457160746	SWT-2.3-93
55.5648139743	7.5543350893	SWT-2.3-93	55.5650323455	7.5629697295	SWT-2.3-93
55.5652411261	7.5716048018	SWT-2.3-93	55.5654492988	7.5802399760	SWT-2.3-93
55.5656658464	7.5888749296	SWT-2.3-93	55.5658728033	7.5975103084	SWT-2.3-93
55.5727349986	7.5455424631	SWT-2.3-93	55.5726306208	7.5541906636	SWT-2.3-93
55.5725254466	7.5628229744	SWT-2.3-93	55.5724288318	7.5714707775	SWT-2.3-93
55.5723134573	7.5801033424	SWT-2.3-93	55.5722156229	7.5887510768	SWT-2.3-93
55.5721080138	7.5973832442	SWT-2.3-93	55.580858953	7.5463050104	SWT-2.3-93
55.5804395759	7.5549189734	SWT-2.3-93	55.5800195926	7.5635327630	SWT-2.3-93
55.5795990029	7.5721463789	SWT-2.3-93	55.5791778070	7.5807598207	SWT-2.3-93
55.5787560049	7.5893730881	SWT-2.3-93	55.5783335966	7.5979861808	SWT-2.3-93
55.5889311015	7.5480059552	SWT-2.3-93	55.5881962871	7.5565539084	SWT-2.3-93
55.5874608749	7.5651015520	SWT-2.3-93	55.5867338477	7.5736485601	SWT-2.3-93
55.58599724	7.5821955857	SWT-2.3-93	55.5852600347	7.5907423010	SWT-2.3-93
55.5845222317	7.5992887055	SWT-2.3-93	55.5969238981	7.5505992712	SWT-2.3-93
55.5958821965	7.5590490670	SWT-2.3-93	55.594839910	7.5674984244	SWT-2.3-93
55.5937970386	7.5759473432	SWT-2.3-93	55.5927535824	7.5843958231	SWT-2.3-93
55.5917005587	7.5928441853	SWT-2.3-93	55.590655933	7.6012917847	SWT-2.3-93
55.6048107156	7.5541182153	SWT-2.3-93	55.6034616958	7.5624379901	SWT-2.3-93
55.6021119233	7.5707413363	SWT-2.3-93	55.600761769	7.5790599867	SWT-2.3-93
55.5994108642	7.5873622090	SWT-2.3-93	55.5980505928	7.5956800550	SWT-2.3-93
55.5966987367	7.6039970149	SWT-2.3-93	55.6125549872	7.5585170259	SWT-2.3-93
55.6108980413	7.5666590013	SWT-2.3-93	55.6092497178	7.5748158413	SWT-2.3-93
55.6075916815	7.5829564603	SWT-2.3-93	55.6059420836	7.5910960783	SWT-2.3-93
55.6042919413	7.5992350207	SWT-2.3-93	55.6026322719	7.6073736057	SWT-2.3-93
55.6201117081	7.5637978210	SWT-2.3-93	55.6181735541	7.5717449287	SWT-2.3-93
55.6162257137	7.5796757120	SWT-2.3-93	55.6142775385	7.5876215870	SWT-2.3-93
55.612328662	7.5955508105	SWT-2.3-93	55.6103704659	7.6034954433	SWT-2.3-93
55.608429716	7.6114386564	SWT-2.3-93	55.6274714146	7.5699296123	SWT-2.3-93
55.6252334968	7.5776346435	SWT-2.3-93	55.6230040723	7.5853384789	SWT-2.3-93
55.6207741585	7.5930414457	SWT-2.3-93	55.6185347726	7.6007438638	SWT-2.3-93
55.6163038805	7.6084450914	SWT-2.3-93	55.6140635165	7.6161457665	SWT-2.3-93
55.6345799014	7.5768988648	SWT-2.3-93	55.6320777563	7.5843284864	SWT-2.3-93
55.6295661724	7.5917574881	SWT-2.3-93	55.6270543138	7.5992014208	SWT-2.3-93
55.6245418172	7.6066285304	SWT-2.3-93	55.6220288648	7.6140546944	SWT-2.3-93
55.6195154569	7.6214799129	SWT-2.3-93	55.6414185134	7.5846589057	SWT-2.3-93
55.6386519422	7.5917969434	SWT-2.3-93	55.635875785	7.5989184190	SWT-2.3-93
55.6330904054	7.6060550890	SWT-2.3-93	55.6303225699	7.6131901154	SWT-2.3-93
55.6275451513	7.6203085781	SWT-2.3-93	55.624758508	7.6274422273	SWT-2.3-93
55.647977938	7.5931944307	SWT-2.3-93	55.644937406	7.5999932439	SWT-2.3-93
55.6419144558	7.6067903682	SWT-2.3-93	55.6388821393	7.6135867651	SWT-2.3-93
55.6358404564	7.6203824300	SWT-2.3-93	55.6328165337	7.6271922949	SWT-2.3-93
55.6297830663	7.6339855478	SWT-2.3-93			

Table A.0.2: Turbine positions and type of turbine in the Horns Rev 2 offshore wind farm.